

Instantaneous frequencies in the Kuramoto model

Julio D. da Fonseca,¹ Edson D. Leonel,¹ and Hugues Chaté^{2,3,4}

¹*Departamento de Física, Universidade Estadual Paulista, Bela Vista, 13506-900 Rio Claro, SP, Brazil*

²*Service de Physique de l'Etat Condensé, CEA, CNRS Université Paris-Saclay, CEA-Saclay, 91191 Gif-sur-Yvette, France*

³*Computational Science Research Center, Beijing 100094, China*

⁴*Sorbonne Université, CNRS, Laboratoire de Physique Théorique de la Matière Condensée, 75005 Paris, France*

(Dated: August 11, 2020)

Using the main results of the Kuramoto theory of globally coupled phase oscillators combined with methods from probability and generalized function theory in a geometric analysis, we extend Kuramoto's results and obtain a mathematical description of the instantaneous frequency (phase-velocity) distribution. Our result is validated against numerical simulations, and we illustrate it in cases where the natural frequencies have normal and Beta distributions. In both cases, we vary the coupling strength and compare systematically the distribution of time-averaged frequencies (a known result of Kuramoto theory) to that of instantaneous frequencies, focussing on their qualitative differences near the synchronized frequency and in their tails. For a class of natural frequency distributions with power-law tails, which includes the Cauchy-Lorentz distribution, we analyze rare events by means of an asymptotic formula obtained from a power series expansion of the instantaneous frequency distribution.

I. INTRODUCTION

In large ensembles of interacting oscillatory units, order emerges when a group starts showing the same frequency. This frequency adjustment, called synchronization [1], is a crucial and ubiquitous phenomenon in many areas of science, such as neurosciences [2], semiconductor laser arrays [3], cardiac pacemaker cells [4], power grids [5], cell metabolism [6], Josephson junction arrays [7], and chemical oscillators [8].

Arthur Winfree was the first to present a theoretical description of synchronization in a model of biological oscillators [9]. Influenced by Winfree's work, Yoshiki Kuramoto introduced his famous minimal model of coupled oscillators [10] and its mathematical analysis [11–14]. Together these seminal works occupy a prominent place in synchronization research. Since Kuramoto's early works, a large number of Kuramoto-like models appeared in later studies discussing effects such as those resulting from phase shifts in the coupling function [15], noise [16], periodic external fields [17], higher modes [18], finite size [19], and complex coupling networks [20].

The Kuramoto model consists in an infinitely large ensemble of oscillators coupled globally. The oscillators are reduced to their phase, they are characterized by their individual natural frequency, and their dynamics is first-order in time. The remarkable discovery of Kuramoto is that when coupled strongly-enough, the oscillators can overcome their nominal frequency quenched disorder and synchronize.

Kuramoto showed that his model exhibits a transition between an incoherent state, where instantaneous frequencies are completely desynchronized, and a partially synchronized state, in which some oscillators share the same instantaneous frequency, and are thus phase locked. The theoretical framework developed by Kuramoto to analyze his model, hereafter "Kuramoto theory", comprises a set of assumptions and analytical results describing sta-

tionary collective states [21]. Kuramoto assumed that these states would be characterized by phase distributions [30] with stationary profiles. These profiles might be uniform (incoherent state) or be a steadily rotating traveling wave profile (synchronized state).

The most common characterization of synchronization in the Kuramoto model is, however, not in terms of phase distributions but simply in terms of a scalar order parameter (which is zero in the incoherent state and takes finite values when oscillators synchronize). Here we pursue yet another, finer, description in terms of the *distribution of instantaneous frequencies*. Although synchronization is a direct manifestation of the way instantaneous frequencies are distributed, this problem was not, to our knowledge, addressed so far. Not even by Kuramoto, who instead solved the problem of the distribution of "coupling-modified frequencies" [11, 12], i.e. instantaneous frequencies averaged over an infinitely long time.

The main goal of this paper is to extend Kuramoto theory by presenting a detailed derivation of the instantaneous frequency distribution without any time-averaging procedure. Our work is essentially based on Kuramoto results and provides a mathematical description of the instantaneous frequency distribution in stationary states, whether incoherent or with synchronized oscillators.

This paper is structured as follows. In Section II we briefly discuss important aspects of Kuramoto theory, including the Kuramoto model, the order parameter, phase distributions of synchronized and desynchronized oscillators, and the distribution of time-averaged frequencies. In Section III, results from Kuramoto theory, together with methods from probability and generalized function theory, are used to develop a geometric analysis that solves the problem of the instantaneous frequency distribution. In Section IV, we illustrate the properties of this distribution in two cases: in the first one, we consider the classic case of an unbounded normal distribution of natural frequencies; in the second, we adopt a symmet-

ric Beta distribution of natural frequencies, defined on a bounded interval. In Section V, we obtain a power series expansion of the instantaneous frequency distribution and an asymptotic formula, which allow us to study rare events (large instantaneous frequency occurrences) in cases where the natural frequency distribution has power-law tails, e.g., Cauchy-Lorentz distributions. Our conclusions and open problems left for further investigation are presented in Sec. VI. In the Appendix, the formula of the instantaneous frequency distribution is compared to instantaneous frequency histograms obtained from numerical simulations of the Kuramoto model.

II. KURAMOTO THEORY

In this section we present some results from the theoretical framework developed by Kuramoto to analyze his coupled oscillator model. For details about how these results can be obtained we refer the reader to Refs. [11, 21].

The Kuramoto model consists of an ensemble of N all-to-all coupled oscillators with randomly distributed natural frequencies ω_i ($i = 1, 2, \dots, N$) whose phases θ_i evolve according to:

$$\dot{\theta}_i = \omega_i + \frac{K}{N} \sum_{j=1}^N \sin(\theta_j - \theta_i), \quad (1)$$

where K is the coupling strength. In Kuramoto theory, N is assumed to be a infinitely large number and the natural frequencies ω_i are randomly distributed according to a given probability density function $g(\omega)$.

Collective states in the Kuramoto model are usually analyzed by using measures which quantify the level of synchronization. One such quantity, proposed by Kuramoto, is

$$R = \lim_{N \rightarrow +\infty} \left| \frac{1}{N} \sum_{j=1}^N \exp(i\theta_j) \right|, \quad (2)$$

which we call here order parameter. If the oscillator state is represented by $\exp(i\theta)$, R is the magnitude of a complex number representing the mean state of oscillators. A fundamental surmise in Kuramoto's theory is that stationary collective states, when they exist, are characterized by time-independent values of the order parameter reached after sufficiently long time. This is equivalent to the assumption that the distribution of phases has a well-defined, steady profile. In an ordered state, the synchronized oscillators adopt a common frequency denoted Ω hereafter.

In order to simplify notations, from here on we use the definitions

$$a = KR \quad \text{and} \quad \tilde{\chi} = \frac{\chi - \Omega}{a}, \quad (3)$$

where χ is a generic quantity.

Kuramoto's analysis considers the use of a frame rotating with angular velocity equal to Ω . The dynamics of an oscillator of natural frequency ω can then be written

$$\dot{\psi} = \omega - \Omega - a \sin \psi, \quad (4)$$

where $\dot{\psi} = \dot{\theta} - \Omega$ and $\psi = \theta - \Omega t$ are descriptions in the rotating frame of the oscillator's instantaneous frequency $\dot{\theta}$ and phase θ .

As Kuramoto did in his early works, here we distinguish two groups of oscillators: synchronized and desynchronized oscillators. Synchronized oscillators are those whose natural frequencies satisfy $|\tilde{\omega}| \leq 1$, which means that (4) has a stable fixed point given by

$$\psi^*(\omega) = \arcsin(\tilde{\omega}). \quad (5)$$

Desynchronized oscillators have natural frequencies such that $|\tilde{\omega}| > 1$. In this case, Eq. (4) has no fixed point: phases show oscillatory dynamics, which look like relaxation oscillations: they change rapidly at some stage of their period, then evolve much more slowly for the rest of the cycle (see Fig. 1(b) for some examples).

According to Eq. (4), if $R = 0$, instantaneous and natural frequencies are the same. For heterogeneous natural frequencies, $R = 0$ characterizes the incoherent state, where oscillators are out of synchrony. Assuming that the natural frequency distribution, g , is symmetric and unimodal, as Kuramoto does in his early works, then Ω coincides with the center of symmetry of g . When oscillators synchronize, the order parameter has a positive value $R = \frac{a}{K}$, obtained by finding the value of a which solves

$$K \int_{-\frac{\pi}{2}}^{+\frac{\pi}{2}} d\psi g(\Omega + a \sin \psi) \cos^2 \psi = 1. \quad (6)$$

Eq. (6) can be used if the assumption of a symmetric and unimodal g holds. For more general profiles, the order parameter has to be computed using a more general (and more difficult to solve) equation whose solution is defined in terms of both a and Ω (see Ref. [15]). In this paper, our analytical results do not depend on how a is computed or on any specific assumption about g . However, we will here consider Eq.(6) in the numerical examples, since it is simpler and more widely known [31].

If g is symmetric and unimodal, the critical coupling strength, i.e. the value of K marking the transition between the desynchronized and the partially synchronized states, is given by

$$K_c = \frac{2}{\pi g(\Omega)}, \quad (7)$$

Again, a more general expression has to be used for more general forms of g [15].

Let $p(\psi, \omega)$ denote the joint probability density involving the oscillator's phase in the rotating frame and

the oscillator's natural frequency. Applying Bayes' rule, $p(\psi, \omega)$ can be expressed

$$p(\psi, \omega) = p(\psi|\omega)g(\omega), \quad (8)$$

where $p(\psi|\omega)$ is the conditional phase density for a given natural frequency ω .

A detailed discussion about how to obtain the conditional density $p(\psi|\omega)$ can be found in Ref. [21]. Here we only show $p(\psi|\omega)$ in its final possible forms. For $|\tilde{\omega}| \leq 1$,

$$p(\psi|\omega) = \delta[\psi - \psi^*(\omega)], \quad (9)$$

where $\psi^*(\omega)$ is the stable fixed point of Eq. (4), given by Eq. (5). For $|\tilde{\omega}| > 1$, Eq. (4) has no fixed point, and the density $p(\psi|\omega)$ can be written as

$$p(\psi|\omega) = \frac{\omega - \Omega}{2\pi\dot{\psi}} \sqrt{1 - \frac{1}{\tilde{\omega}^2}}, \quad (10)$$

where $\dot{\psi}$ is given by Eq. (4).

From formulas equivalent to Eqs. (9) and (10), Kuramoto obtained the phase distribution, given by

$$n(\psi) = n_S(\psi) + n_D(\psi), \quad (11)$$

where $n_S(\psi)$, the phase distribution of synchronized oscillators, is

$$n_S(\psi) = \begin{cases} g(\Omega + a \sin \psi) a \cos \psi, & |\psi| \leq \frac{\pi}{2} \\ 0, & |\psi| > \frac{\pi}{2} \end{cases} \quad (12)$$

and $n_D(\psi)$ denotes the phase distribution of desynchronized oscillators, given by

$$n_D(\psi) = \frac{1}{2\pi} \int_{|x|>a} \frac{xg(\Omega + x)}{x - a \sin \psi} \sqrt{1 - \left(\frac{a}{x}\right)^2} dx. \quad (13)$$

For $R > 0$, the phase distribution profile shape is fixed and travels a distance of Ωt during a time interval t in the non-rotating frame (where phases are described by θ). This is the scenario with synchronized oscillators: a phase distribution as a steadily traveling wave. In the incoherent state, $R = 0$, whence, according to Eqs. (12) and (13), phases are uniformly distributed, viz., $n(\psi) = \frac{1}{2\pi}$.

Kuramoto also obtained the distribution of "coupling-modified frequencies" [11, 12], which are the instantaneous frequencies averaged over an infinitely long time, as thoroughly discussed in Ref. [21]. The infinite-time average $\bar{\omega}$ of an oscillator's instantaneous frequency $\dot{\theta}$, can be defined as

$$\bar{\omega} = \lim_{T \rightarrow +\infty} \frac{1}{T} \int_0^T \dot{\theta}(t) dt. \quad (14)$$

Kuramoto showed that the coupling-modified frequencies are distributed accordingly to

$$\bar{G}(\nu) = \delta(\nu - \Omega) S(K) + \bar{G}_D(\nu), \quad (15)$$

where

$$S(K) = \int_{\Omega-a}^{\Omega+a} g(\omega) d\omega, \quad (16)$$

$$\bar{G}_D(\nu) = \frac{|\tilde{\nu}|}{\sqrt{1 + \tilde{\nu}^2}} g\left(\Omega + \frac{\nu - \Omega}{|\tilde{\nu}|} \sqrt{1 + \tilde{\nu}^2}\right) \quad (17)$$

for $\nu \neq \Omega$, and $\bar{G}_D(\Omega) = 0$.

Equation (15) states that: (i) $\bar{G}(\nu)$ exhibits a singularity at the synchronization frequency Ω ; (ii) $\bar{G}(\nu)$ goes linearly to zero for ν near Ω ; and (iii) $\lim_{\epsilon \rightarrow 0^+} \int_{\Omega-\epsilon}^{\Omega+\epsilon} \bar{G}(\nu) d\nu = S(K)$, i.e. the probability of an oscillator having a time-averaged frequency arbitrarily near Ω is given by $S(K)$, which represents the fraction of synchronized oscillators.

Figure 1 summarizes these findings, together with some numerical illustration of the object of central interest here, the distribution of instantaneous frequencies. In Figs. 1(a) and (b) we show time series of the instantaneous frequencies of eight oscillators selected from a total ensemble of $N = 5 \times 10^5$ oscillators with their natural frequencies distributed according to a normal (Gaussian) distribution centered at $\Omega = 0$. For this case $K_c \simeq 1.5957$. In Fig. 1(a), we set $K = 0.8 < K_c$ in the desynchronized regime ($a = 0$), and all oscillators quickly keep their natural frequency. In Fig. 1(b), $K = 1.8 > K_c$, in the synchronized regime ($a > 0$): the 4 oscillators with their natural frequency $|\tilde{\omega}| < 1$ synchronize to $\Omega = 0$, while the others stay desynchronized and their instantaneous frequencies exhibit relaxation-oscillation-like dynamics.

In Figs. 1(c) and (d) we use the same K values as in (a) and (b) and show: i) g the Gaussian distribution of natural frequencies; ii) \bar{G}_D the continuous part of the distribution of time-averaged instantaneous frequencies given by Eq. (17); and iii) numerically-determined normalized histograms of instantaneous frequencies (see Appendix for details). As expected, all these distributions coincide in the subcritical case shown in Fig. 1(c). For $K = 1.8 > K_c$ (Fig. 1(d)), the histogram of instantaneous frequencies shows a peak located at $\Omega = 0$ which correspond to the synchronized oscillators. Note that the instantaneous frequencies (shown in the histogram) are distributed in a qualitatively different way from their time-averaged counterparts. Remarkable differences are the accumulation of desynchronized oscillators' instantaneous frequencies near zero and the fact that the tails of the instantaneous frequency distribution are "fatter" than those of the time-averaged and nominal frequencies.

Coming back to the periodic dynamics of individual desynchronized oscillators in the synchronized regime

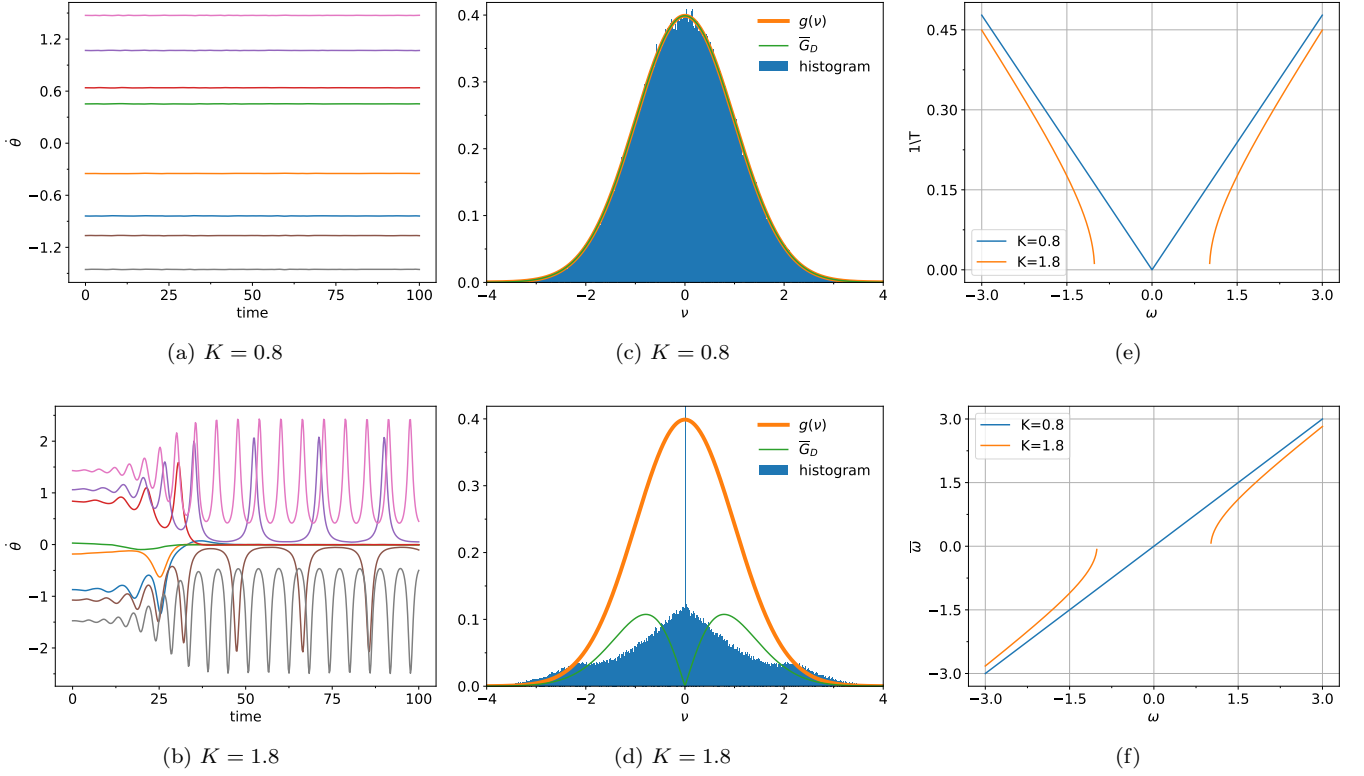


FIG. 1. (a) Time-series of instantaneous frequencies for $K < K_c$. (b) Same as (a), but for $K > K_c$. (c) g and \bar{G}_D compared to normalized histograms of instantaneous frequencies. (d) Same as (c), but for $K > K_c$. (e) Oscillation frequency, i.e. number of phase-cycles per time unit (T^{-1}), defined by Eq.(18). (f) Time-averaged instantaneous frequency ($\bar{\omega}$), defined by Eq. (19). Numerical results were obtained using a normal distribution of natural frequencies and a number of oscillators $N = 5 \times 10^5$. See Appendix for numerical details.

(Fig. 1(b)), we see from Eq. (4) that the amplitude of oscillations of $\dot{\theta}$ is a , and the minimum and maximum values reached are $\dot{\theta}_{min} = \omega - a$ and $\dot{\theta}_{max} = \omega + a$, so that the middle value is the natural frequency of the oscillator. As discussed in Ref. [21], a desynchronized oscillator's phase makes a complete 2π turn during a time-interval $T(\omega)$, which is given by

$$T(\omega) = \frac{2\pi}{\sqrt{(\omega - \Omega)^2 - a^2}}. \quad (18)$$

The time-averaged instantaneous frequency, defined by (14), can be given in terms of T as

$$\bar{\omega} = \begin{cases} \Omega + \frac{2\pi}{T}, & \omega > \Omega + a \\ \Omega - \frac{2\pi}{T}, & \omega < \Omega - a. \end{cases} \quad (19)$$

If $a = 0$, we can write (18) and (19) as $\frac{1}{T} = \frac{|\omega - \Omega|}{2\pi}$, and $\bar{\omega} = \omega$. If $a > 0$, (18) is the same as $\frac{1}{T} = \frac{a}{2\pi} \sqrt{\tilde{\omega}^2 - 1}$, and (19) can be written as $\bar{\omega} = \Omega \pm a\sqrt{\tilde{\omega}^2 - 1}$ for $\pm\tilde{\omega} > 1$.

These formulas allow us to infer the following properties of the instantaneous frequency of non-synchronized oscillators: i) as $\tilde{\omega} \rightarrow \pm 1^\pm$, we have $\frac{1}{T} \rightarrow 0$, which means slow oscillations, or oscillations with large-time periods;

ii) if $\tilde{\omega} \rightarrow 1^+$, then $\bar{\omega} \rightarrow \Omega^+$ and $\dot{\theta}_{min} = \omega - a \rightarrow \Omega^+$, i.e. both the time-averaged and minimum instantaneous frequencies have values close to and greater than Ω , the frequency of synchronized oscillators (Similar properties are of course valid if $\tilde{\omega} \rightarrow 1^-$); iii) as $|\tilde{\omega}| \rightarrow \infty$, then we have $\frac{1}{T} \rightarrow \infty$ and $\bar{\omega} \rightarrow \omega$, viz. fast oscillations with time-averages becoming close to their oscillation centers.

Fig. 1(b) illustrates all these properties. The long periods of time spent near Ω by the instantaneous frequency of oscillators with $|\tilde{\omega}| \gtrsim 1$ explains why the histogram in Fig. 1(d) exhibits frequent occurrences near zero.

Figs. 1(e) and (f) show plots of $\frac{1}{T}$ and $\bar{\omega}$ as functions of ω created using Eqs. (18) and (19). The synchronized frequency Ω has been set to zero and we adopted the same values of K as used in Figs.1(a)-(d). For $K = 0.8$ ($a = 0$), the graphs are shown in blue. The curves in orange correspond to the case where $K = 1.8$ ($a \simeq 1$).

In summary, many of the properties shown in Fig. 1 are straight consequences of Kuramoto theory. Those regarding instantaneous frequencies can be qualitatively explained by it. This is the case of the accumulation of instantaneous frequencies near the synchronization frequency (Fig. 1(d)). We now proceed to the core of this work, which is the calculation of the full analytical expression of the distribution of instantaneous frequencies.

III. DISTRIBUTION OF INSTANTANEOUS FREQUENCIES

Our goal in this section is to obtain, based on the results discussed in Section II, the distribution of instantaneous frequencies in the Kuramoto model. This distribution is a probability density function $G(\nu)$, which means that $G(\nu) d\nu$ is the probability of an oscillator showing its fixed frame instantaneous frequency, $\dot{\theta}$, in the interval $[\nu, \nu + d\nu]$.

By using the random variable transformation theorem [24], we have

$$G(\nu) = \int_{-\infty}^{+\infty} \int_{-\pi}^{+\pi} \delta[\nu - \dot{\theta}(\omega, \psi)] p(\psi, \omega) d\psi d\omega, \quad (20)$$

where δ denotes the delta function, $\dot{\theta}(\omega, \psi)$ is a random variable transformation, given by

$$\dot{\theta}(\omega, \psi) = \omega - a \sin \psi, \quad (21)$$

and $p(\psi, \omega)$ is the joint probability density involving the phase in the rotating frame and the natural frequency. Equation (21) comes from Eq.(4), which describes instantaneous frequencies in the rotating frame.

The delta function in Eq. (20), $\delta[\nu - \dot{\theta}(\omega, \psi)]$, is concentrated in a curve embedded in the two-dimensional space defined by the integration variables ψ and ω . In order to calculate the double integral in Eq. (20), we use a method proposed by Seeley [25, 26], which generalizes the usual concept of one-dimensional delta functions to delta functions concentrated in manifolds with an arbitrary number of dimensions.

Let $\delta(P)$ denote a delta function concentrated in a $n-1$ -dimensional manifold M embedded in a n -dimensional space V . The manifold M is defined by $P(\mathbf{x}) = 0$, where $P(\mathbf{x})$ is a function at $\mathbf{x} = (x_1, \dots, x_n)$, i.e. a point in V with coordinates x_1, \dots, x_n . The delta function $\delta(P)$ can be defined by

$$\delta(P) = \lim_{c \rightarrow 0^+} \frac{\Theta(P+c) - \Theta(P)}{c}, \quad (22)$$

where $\Theta(\cdot)$ is a Heaviside step function such that $\Theta(P) = 1$ for $P \geq 0$, and $\Theta(P) = 0$ for $P < 0$.

Consider a function $\varphi(\mathbf{x})$ defined in V . From Eq. (22), we have

$$\int_V \delta(P) \varphi(\mathbf{x}) d^n \mathbf{x} = \lim_{c \rightarrow 0^+} \int_{-c \leq P < 0} \frac{\varphi(\mathbf{x})}{c} d^n \mathbf{x}, \quad (23)$$

where $d^n \mathbf{x} = dx_1 \dots dx_n$.

Let γ be the distance between the manifolds $M_{P=0}$ and $M_{P=-c}$, defined by the equations $P = 0$ and $P = -c$, respectively. Then, for $P(\mathbf{x}) = 0$, we have $P[\mathbf{x} + \gamma \hat{n}(\mathbf{x})] = -c$, i.e., if $\mathbf{x} \in M_{P=0}$, then $\mathbf{x} + \gamma \hat{n}(\mathbf{x}) \in M_{P=-c}$, where $\hat{n}(\mathbf{x})$ is the unit vector normal to $M_{P=0}$ at \mathbf{x} . As

$c \rightarrow 0^+$, a first-order expansion of $P[\mathbf{x} + \gamma \hat{n}(\mathbf{x})]$ results in $P(\mathbf{x}) - \gamma \hat{n} \cdot \nabla P = -c$, from which we obtain

$$\gamma = \frac{c}{|\nabla P|}, \quad (24)$$

since $P(\mathbf{x}) = 0$ and $\hat{n}(\mathbf{x}) = \frac{\nabla P}{|\nabla P|}$.

Changing the infinitesimal volume element $d^n \mathbf{x}$ by γdS , where γ is given by Eq. (24) and dS is an infinitesimal surface element of $M_{P=0}$, Eq. (23) can be rewritten as

$$\int_V \delta(P) \varphi(\mathbf{x}) d^n \mathbf{x} = \int_{M_{P=0}} \frac{\varphi(\mathbf{x})}{|\nabla P|} dS, \quad (25)$$

which means that the volume integral in the right-side of Eq. (23) can be changed by a surface integral on $M_{P=0}$.

Suppose that $M_{P=0}$ is a curve, and V , a two-dimensional space. In this particular case, Eq. (25) can be written in the form

$$\int_V \delta[P(\mathbf{x})] \varphi(\mathbf{x}) d^2 \mathbf{x} = \int_{M_{P=0}} \frac{\varphi(\mathbf{x})}{|\nabla P|} dl, \quad (26)$$

where $\mathbf{x} = (x_1, x_2)$, $d^2 \mathbf{x} = dx_1 dx_2$, and dl is an infinitesimal line element of $M_{P=0}$. Let $P(x_1, x_2)$ be defined by $P(x_1, x_2) = f(x_1) - x_2$, where $f(x_1)$ is a continuous function, and the range of x_1 is the interval $[a, b]$. Then, the curve $M_{P(x_1, x_2)=0}$ is the graph of $x_2 = f(x_1)$ with $a \leq x_1 < b$. Suppose that C_M is a curve corresponding to a part of $M_{P(x_1, x_2)=0}$. This curve can be defined as a subset of $M_{P(x_1, x_2)=0}$ by $C_M = \{(x_1, x_2) \in V \mid x_2 = f(x_1) \text{ and } \psi_a \leq x_1 \leq \psi_b < b\}$. An integral along C_M , analogous to the right-hand side of Eq. (26), can be written as

$$\int_C \frac{\varphi(x_1, x_2)}{|\nabla P(x_1, x_2)|} dl = \int_{\psi_a}^{\psi_b} \varphi[x_1, f(x_1)] dx_1. \quad (27)$$

We are now able to compute the right-hand side of Eq. (20). Let us first put Eq. (20) in the form

$$G(\nu) = \int_V \delta[P_\nu(\psi, \omega)] p(\psi, \omega) d\psi d\omega, \quad (28)$$

where the integration manifold, V , is an infinite-length cylinder $V = [-\frac{\pi}{2}, +\frac{3\pi}{2}] \times (-\infty, +\infty)$, $P_\nu(\psi, \omega)$ is given by

$$P_\nu(\psi, \omega) = F_\nu(\psi) - \omega, \quad (29)$$

with

$$F_\nu(\psi) = a \sin \psi + \nu, \quad (30)$$

and $-\frac{\pi}{2} \leq \psi < +\frac{3\pi}{2}$.

Then, $M_{P_\nu=0}$ is a closed curve in V defined by

$$M_{P_\nu=0} = \{(\psi, \omega) \in V \mid \omega = F_\nu(\psi)\}. \quad (31)$$

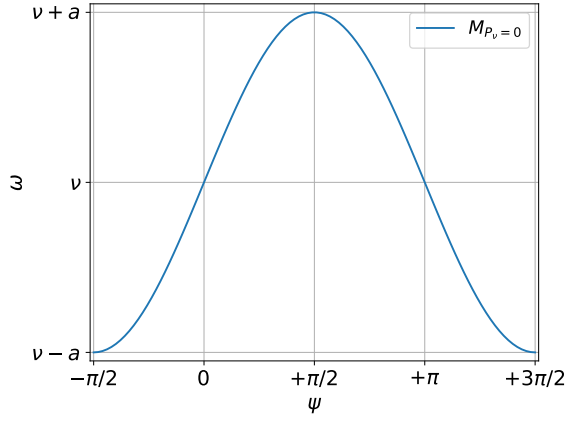


FIG. 2. Graph of F_ν , Eq. (30), representing the curve $M_{P_\nu=0}$, Eq. (31). The minimum is $(-\frac{\pi}{2}, \nu - a)$, and the point of maximum is $(+\frac{\pi}{2}, \nu + a)$.

This curve is represented by the graph of F_ν , shown in Fig. 2. The position of the curve $M_{P_\nu=0}$ in the integration manifold V is determined by the value of ν , which is the argument of G . And the height of $M_{P_\nu=0}$, as shown in Fig. 2, is $2a$. The curve shifts by varying ν and stretches as the product a increases.

Using the relation (26), we obtain from Eq. (28) the formula

$$G(\nu) = \int_{M_{P_\nu=0}} \frac{p(\psi, \omega)}{|\nabla P_\nu(\psi, \omega)|} dl. \quad (32)$$

We can calculate the line integral in Eq. (32) by use of a geometric analysis based on dividing V in two disjoint regions, $V_S = [-\frac{\pi}{2}, +\frac{3\pi}{2}] \times [-a + \Omega, \Omega + a]$ and $V_D = V - V_D$. A sketch of both regions and $M_{P_\nu=0}$ in different locations is shown in Figs.3(a)-(e). Depending on the location and height of $M_{P_\nu=0}$, this curve is completely inside V_D (Figs. 3 (a) and (e)) and can also be partly or entirely in V_S (Figs. 3(b),(c) and (d)). We denote the parts in V_D by $M_{P_\nu=0}^D$, which are the blue curves, and those in V_S by $M_{P_\nu=0}^S$, represented by the yellow curves.

Using Eq. (8), we have that Eq. (32) is the same as

$$G(\nu) = G_S(\nu) + G_D(\nu), \quad (33)$$

where

$$G_S(\nu) = \int_{M_{P_\nu=0}^S} \frac{p(\psi|\omega)g(\omega)}{|\nabla P_\nu(\psi, \omega)|} dl, \quad (34)$$

and

$$G_D(\nu) = \int_{M_{P_\nu=0}^D} \frac{p(\psi|\omega)g(\omega)}{|\nabla P_\nu(\psi, \omega)|} dl. \quad (35)$$

If $M_{P_\nu=0}$ has no part inside V_s , then the curve $M_{P_\nu=0}^S$ does not exist and $G_S(\nu) = 0$. Similarly, if $M_{P_\nu=0}^D$ is an empty set, then we also have $G_D(\nu) = 0$.

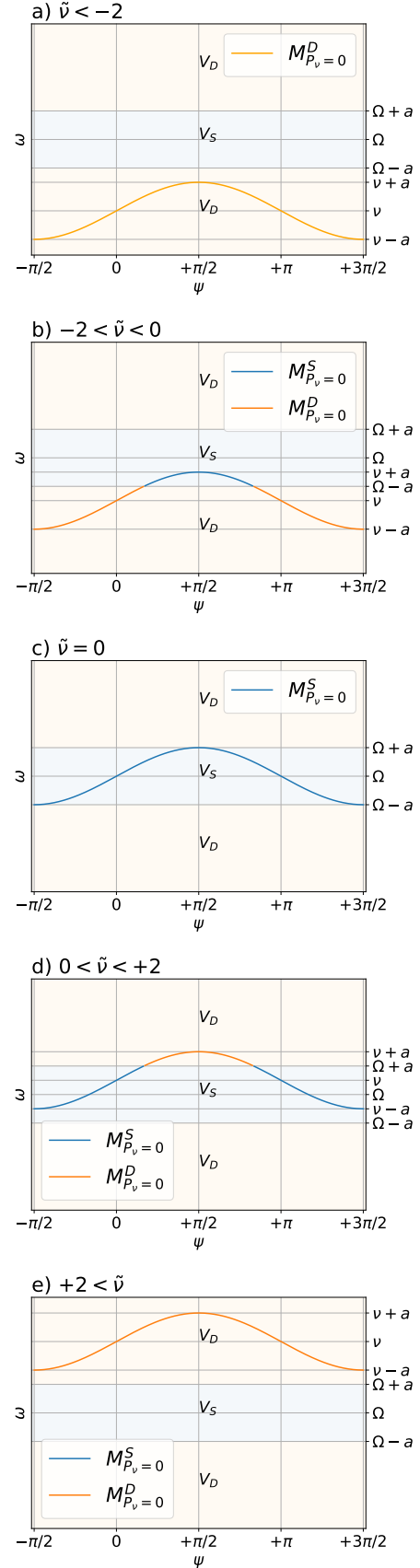


FIG. 3. The curve $M_{P_\nu=0}$ in different locations depending on the value of ν . The part of $M_{P_\nu=0}$ immersed in V_D is $M_{P_\nu=0}^D$, and the intersection between $M_{P_\nu=0}$ and V_S is $M_{P_\nu=0}^S$.

	$-2 < \tilde{\nu} \leq 0$	$0 < \tilde{\nu} < +2$
$\psi_1^S(\nu)$	$-\arcsin(1 + \tilde{\nu})$	$-\frac{\pi}{2}$
$\psi_2^S(\nu)$	$+\frac{\pi}{2}$	$\arcsin(1 - \tilde{\nu})$

TABLE I. Integration limits of Eq. (37), given by $\psi_1^S(\nu)$ and $\psi_2^S(\nu)$. For $|\tilde{\nu}| \geq 2$, $\psi_1^S(\nu)$ and $\psi_2^S(\nu)$ are not defined, and $G_S(\nu) = 0$.

We consider first the case in which $M_{P_\nu=0}^S$ exists. A point (ψ, ω) in $M_{P_\nu=0}^S$ satisfies the conditions: i) $\omega = F_\nu(\psi)$; ii) $-a + \Omega \leq \omega \leq \Omega + a$, as can also be seen in Figs. 3(b),(c) and (d). Condition ii) means that the density $p(\psi|\omega)$ in Eq. (34) is defined by Eq. (9). Then

$$G_S(\nu) = \int_{M_{P_\nu=0}^S} \delta[\psi - \psi^*(\omega)] \frac{g(\omega)}{|\nabla P_\nu(\psi, \omega)|} dl, \quad (36)$$

where $\psi^*(\omega)$ is given by Eq. (5). Integration along $M_{P_\nu=0}^S$ can be done in three steps: the first one is integration along $M_{P_\nu=0}^{SL}$, i.e. the subset of $M_{P_\nu=0}^S$ whose projection in the ψ -axis is contained in the closed interval $[-\frac{\pi}{2}, +\frac{\pi}{2}]$; the second step is integration along $M_{P_\nu=0}^{SR}$, which is the subset of $M_{P_\nu=0}^S$ whose projection in the ψ -axis is contained in the open interval $(-\frac{\pi}{2}, +\frac{3\pi}{2})$; the last step consists in summing the results of both integrations. For a point (ψ, ω) in $M_{P_\nu=0}^{SR}$, we have $+\frac{\pi}{2} < \psi < +\frac{3\pi}{2}$ and $-\frac{\pi}{2} \leq \psi^*(\omega) \leq +\frac{\pi}{2}$. Then, $\psi - \psi^*(\omega) > 0$ and $\delta[\psi - \psi^*(\omega)] = 0$, which means that the integral along $M_{P_\nu=0}^{SR}$ is zero, and the integral along $M_{P_\nu=0}^S$ in Eq. (36) reduces to the integral along $M_{P_\nu=0}^{SL}$.

If $M_{P_\nu=0}^{SL}$ is a non-empty set, the projection of $M_{P_\nu=0}^{SL}$ in the ψ -axis can be represented by the interval $[\psi_1^S(\nu), \psi_2^S(\nu)]$, and we can use (27) and (36) to obtain

$$G_S(\nu) = \int_{\psi_1^S(\nu)}^{\psi_2^S(\nu)} \delta\{\psi - \psi^*[F_\nu(\psi)]\} g[F_\nu(\psi)] d\psi, \quad (37)$$

where F_ν is defined by Eq. (30), and the integration limits, $\psi_1^S(\nu)$ and $\psi_2^S(\nu)$, are given in Table I.

For $|\tilde{\nu}| \geq 2$, $\psi_1^S(\nu)$ and $\psi_2^S(\nu)$ are not defined, and $G_S(\nu) = 0$. This case is illustrated by Figs. 3(a) and (e), which show $M_{P_\nu=0}$ entirely outside V_S . The case $-2 < \tilde{\nu} \leq 0$ is related to configurations with $M_{P_\nu=0}$ partly or completely inside V_S , such as those depicted in Figs. 3(b)-(c). When $0 < \tilde{\nu} < +2$, there is still partial embedding of $M_{P_\nu=0}$ in V_S (See Fig. 3(d)).

From the definitions of ψ^* and F_ν (see Eqs. (5) and (30)), the delta function in the integrand of Eq. (37) is given by

$$\delta\{\psi - \psi^*[F_\nu(\psi)]\} = \delta[\psi - \arcsin(\sin \psi + \tilde{\nu})], \quad (38)$$

which is singular when

$$\psi = \arcsin(\sin \psi + \tilde{\nu}). \quad (39)$$

By applying the sine function on both sides of Eq. (39), we see that the singularity occurs if and only if $\nu = \Omega$ independently of the value taken by ψ . So Eq. (38) only makes sense in an integral where ν is the integration variable and will remain as a delta function despite of integration in Eq. (37).

From Eq. (38), $\delta\{\psi - \psi^*[F_\nu(\psi)]\}$ in its Gaussian form reads

$$\delta\{\psi - \psi^*[F_\nu(\psi)]\} = L[\psi - \arcsin(\sin \psi + \tilde{\nu})], \quad (40)$$

where

$$L(x) = \lim_{\epsilon \rightarrow 0^+} \frac{1}{\epsilon\sqrt{\pi}} \exp\left[-\left(\frac{x}{\epsilon}\right)^2\right]. \quad (41)$$

This limit can be analyzed in an arbitrarily small open neighborhood \mathcal{N} of radius ϵ centered in the singularity point, defined by $\nu = \Omega$. As expected for delta functions in non-singular points, if ν is not in \mathcal{N} , i.e. $|\nu - \Omega| \geq \epsilon$, the limit in (40) is zero, since the Gaussian is $O(\epsilon^{2m-1})$ as $\epsilon \rightarrow 0^+$ for any positive integer m . If ν is inside \mathcal{N} , i.e. $|\nu - \Omega| < \epsilon$, then

$$\arcsin(\sin \psi + \tilde{\nu}) = \psi + \frac{\tilde{\nu}}{\cos \psi} + O(\tilde{\nu}^2), \quad (42)$$

for $\epsilon \rightarrow 0^+$. By redefining ϵ as $\epsilon \cos \psi$ and substituting (42) in (40), we obtain

$$\delta\{\psi - \psi^*[F_\nu(\psi)]\} = \cos \psi L(\tilde{\nu}), \quad (43)$$

where $L(\tilde{\nu})$ is the Gaussian representation of $\delta(\tilde{\nu})$. Substituting (43) in (37), we have

$$G_S(\nu) = \delta(\tilde{\nu}) \int_{\psi_2^S(\nu)}^{\psi_1^S(\nu)} g(a \sin \psi + \nu) \cos \psi d\psi, \quad (44)$$

which is the same as

$$G_S(\nu) = a\delta(\nu - \Omega) \int_{-\frac{\pi}{2}}^{+\frac{\pi}{2}} g(a \sin \psi + \Omega) \cos \psi d\psi. \quad (45)$$

Changing the integration variable ψ to $\omega = a \sin \psi + \Omega$, Eq. (45) results in

$$G_S(\nu) = \delta(\nu - \Omega) S(K), \quad (46)$$

where $S(K)$, as mentioned in Sec.II, is the fraction of synchronized oscillators, defined by Eq. (16). It is worth mentioning that $G_S(\nu)$ is identical to the singular term in the distribution of time-averaged frequencies, as shown by Eq. (15).

A similar geometric analysis can be used to calculate $G_D(\nu)$ from Eq. (35), where integration is now performed along the curve $M_{P_\nu=0}^D$. As mentioned before, this curve corresponds to the part of $M_{P_\nu=0}$ in V_D . A point (ψ, ω) in $M_{P_\nu=0}^D$ satisfies the conditions: i) $\omega = F_\nu(\psi)$; ii) $\omega < \Omega - a$ or $\omega > \Omega + a$ (see orange curves in Figs. 3(a),(b),(d), and (e)). From condition i), (30), and (4), we have that

	$\tilde{\nu} \leq -2$	$-2 < \tilde{\nu} < 0$	$0 < \tilde{\nu} < +2$	$+2 \leq \tilde{\nu}$
$\psi_1^D(\nu)$	$-\frac{\pi}{2}$	$-\frac{\pi}{2}$	$\arcsin(1 - \tilde{\nu})$	$-\frac{\pi}{2}$
$\psi_2^D(\nu)$	$+\frac{\pi}{2}$	$-\arcsin(1 + \tilde{\nu})$	$+\frac{\pi}{2}$	$+\frac{\pi}{2}$

TABLE II. Integration limits of Eq. (49), given by $\psi_1^D(\nu)$ and $\psi_2^D(\nu)$. The limits are not defined for $\nu = \Omega$. (49) does not apply, and $G_D(\nu) = 0$.

$\dot{\psi} = \nu - \Omega$. From condition ii), $p(\psi|\omega)$ is defined by (10), and Eq. (35) can then be rewritten as

$$G_D(\nu) = \frac{1}{2\pi\tilde{\nu}} \int_{M_{P\nu=0}^D} \frac{\tilde{\omega}g(\omega)}{|\nabla P_\nu(\psi, \omega)|} \sqrt{1 - \frac{1}{\tilde{\omega}^2}} dl. \quad (47)$$

For $\nu = \Omega$, $M_{P\nu=0}^D$ is an empty set, as shown in Fig. 3(c), and $G_D(\nu) = 0$.

Let $U(x)$ be defined as

$$U(x) = \sqrt{x^2 - 1}. \quad (48)$$

From Eq.(27) and condition i), (47) reads

$$G_D(\nu) = \frac{1}{\pi|\tilde{\nu}|} \int_{\psi_1^D(\nu)}^{\psi_2^D(\nu)} g[F_\nu(\psi)] U[\tilde{F}_\nu(\psi)] d\psi, \quad (49)$$

where $\psi_1^D(\nu)$ and $\psi_2^D(\nu)$ are given in Table II.

As G_S and G_D are given by Eqs. (46) and (51), we can now return to Eq. (33) and write G in its final form:

$$G(\nu) = \delta(\nu - \Omega) S(K) + G_D(\nu), \quad (50)$$

where $G_D(\Omega) = 0$, and

$$G_D(\nu) = \frac{1}{\pi|\tilde{\nu}|} \int_{\psi_\nu^-}^{\psi_\nu^+} h_\nu(\psi) d\psi, \quad (51)$$

if $\nu \neq \Omega$. In Eq. (51), the quantities $h_\nu(\psi)$, χ_ν , ψ_ν^- , and ψ_ν^+ are defined by

$$h_\nu(\psi) = g(a \sin \psi + \nu) U(\sin \psi + \tilde{\nu}) \quad (52)$$

and

$$\psi_\nu^\pm = \arcsin\{- (\tilde{\nu} \pm 2) \Theta[-\tilde{\nu}(\tilde{\nu} \pm 2)] \pm 1\}, \quad (53)$$

where $\Theta[\cdot]$ denotes the Heaviside step function. Note that ψ_ν^- and ψ_ν^+ correspond to the previously defined $\psi_1^D(\nu)$ and $\psi_2^D(\nu)$.

The singular term in (50) means that

$$\lim_{\epsilon \rightarrow 0^+} \int_{\Omega-\epsilon}^{\Omega+\epsilon} G(\nu) d\nu = S(K), \quad (54)$$

i.e. the probability of an oscillator with instantaneous frequency in an infinitesimally small neighborhood of Ω is given by the fraction of synchronized oscillators.

Our procedure to obtain Eq. (50) does not depend in any symmetry assumption related to g . But let us now assume the situation where $g(\Omega + x) = g(\Omega - x)$ for any positive number x . This implies that G has the same property, viz. if $g(\Omega + x) = g(\Omega - x)$, then $G(\Omega + x) = G(\Omega - x)$. To show this, it is sufficient showing that G_D is also symmetric. For $x > 0$, we have

$$G_D(\Omega \pm x) = \frac{a}{\pi x} \int_{\psi_{\Omega \mp x}^-}^{\psi_{\Omega \pm x}^+} h_{\Omega \pm x}(\psi) d\psi, \quad (55)$$

and $\psi_{\Omega \pm x}^- = -\psi_{\Omega \mp x}^+$. In the formula for $G_D(\Omega + x)$ (see Eq. (55)), we can introduce the following changes: first, we change $\psi_{\Omega+x}^-$ by $-\psi_{\Omega-x}^+$ and $\psi_{\Omega+x}^+$ by $-\psi_{\Omega-x}^-$; second, we redefine ψ as $-\psi$. Then,

$$G_D(\Omega + x) = \frac{a}{\pi x} \int_{\psi_{\Omega-x}^-}^{\psi_{\Omega-x}^+} h_{\Omega+x}(-\psi) d\psi', \quad (56)$$

Since $g[\Omega - (a \sin \psi - x)] = g(a \sin \psi + \Omega - x)$ (from the symmetry assumption of g) and $U(-\sin \psi + \frac{x}{a}) = U(\sin \psi - \frac{x}{a})$, we have $h_{\Omega+x}(-\psi) = h_{\Omega-x}(\psi)$. Then, from Eq. (56), $G_D(\Omega + x) = G_D(\Omega - x)$, which proves our initial statement.

According to Eq. (50), G consists of a delta peak and a distribution of instantaneous frequencies for non-synchronized oscillators (G_D). G_D is zero at Ω , where the delta peak is located. \bar{G} has a similar form: the same delta peak at Ω , and a distribution of time-averaged instantaneous frequencies for non-synchronized oscillators (\bar{G}_D). \bar{G}_D is also zero at Ω . Since a synchronized oscillator's instantaneous frequency goes to Ω as time goes to infinity, the same happens to its average in time. This explains why the fraction of synchronized oscillators, defined by $S(K)$, appears as a factor in the delta peaks of both G and \bar{G} .

IV. APPLICATION TO GAUSSIAN AND BETA DISTRIBUTIONS

In this section we illustrate our analytical results about the instantaneous frequency distributions on two distributions of natural frequencies, the normal (Gaussian) distribution and the Beta distribution. Both are unimodal, but one has unbounded support, whereas the other lives on a finite interval (Beta distribution).

A. General features

The Gaussian natural frequency distribution considered is

$$g(\omega) = \frac{1}{\sqrt{2\pi}} \exp\left(-\frac{\omega^2}{2}\right), \quad (57)$$

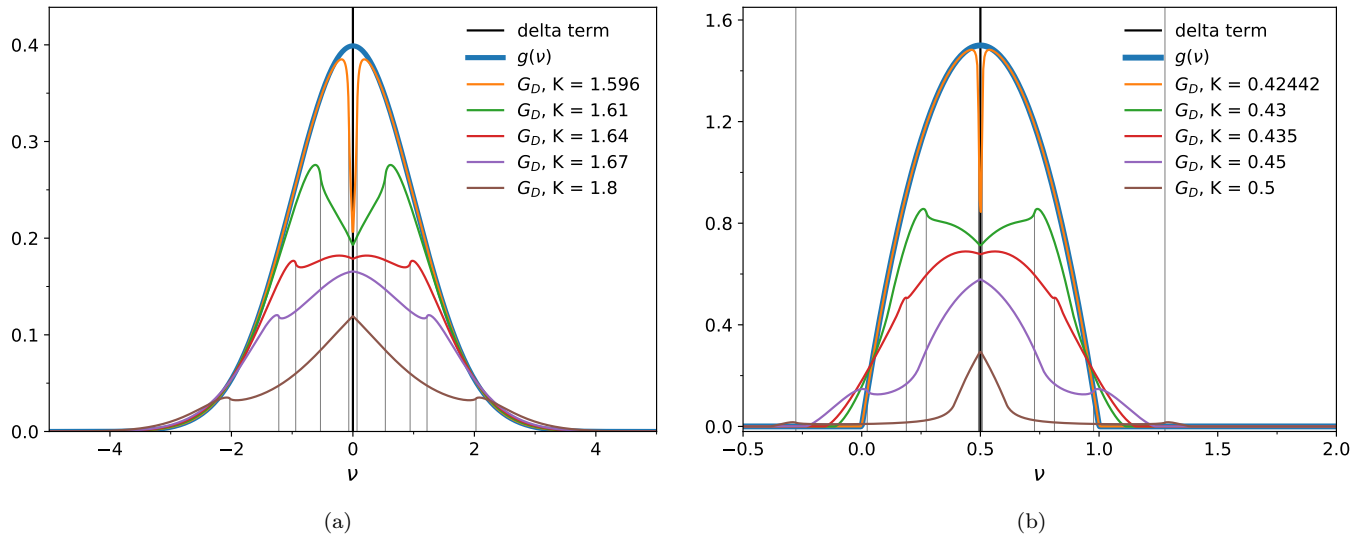


FIG. 4. (a) Instantaneous frequency distribution (G) for natural frequencies normally distributed. The thin vertical lines show different locations of Ω_- and Ω_+ , defined by $\Omega_{\pm} = \Omega \pm 2a$. Fractions of synchronized oscillators ($S(K)$): $S(1.596) = 0.03$; $S(1.61) = 0.21$; $S(1.64) = 0.36$; $S(1.67) = 0.46$; $S(1.8) = 0.69$. (b) Graphs of G assuming a Beta(2,2) distribution of natural frequencies. $S(K)$: $S(0.42442) = 0.01$; $S(0.43) = 0.34$; $S(0.435) = 0.45$; $S(0.45) = 0.66$; $S(0.5) = 0.93$.

for which $\Omega = 0$, and, according to Eq. (7), $K_c \simeq 1.5957$.

The Beta distribution considered reads

$$g(\omega) = \begin{cases} 6\omega(1-\omega) & \omega \in [0, 1] \\ 0 & \omega \notin [0, 1]. \end{cases} \quad (58)$$

which is usually called Beta(2,2). All members of the family of Beta distributions have the support interval $[0, 1]$. So in this example oscillators have no natural frequencies outside the interval $[0, 1]$. Given the symmetric shape, the synchronization frequency is $\Omega = 0.5$. The critical coupling strength, given by Eq. (7), is $K_c \simeq 0.42441$.

In Fig. 4, we show these two distributions (thick blue curves), but also the distribution of instantaneous frequencies for different values of the coupling strength above the critical coupling K_c . (For subcritical coupling values, the instantaneous frequencies are the natural frequencies.) For $K > K_c$, $G(\nu) = G_S(\nu) + G_D(\nu)$, where $G_S(\nu)$ and $G_D(\nu)$ are defined by Eqs. (46) and (51), respectively. Since $G_S(\nu)$ is a Dirac delta term, we represent it by a black vertical line located in Ω .

The thin colored curves show G_D for different values of K . This continuous part of G obeys the symmetry of g , the distribution of natural frequencies. The tails of G_D are fatter than those of g . In particular, G_D extends beyond the interval of support of g in the Beta case. In the central region, $G_D(\nu) < g(\nu)$. For $K \gtrsim K_c$, G_D is very close to g , but for a sharp drop near Ω , the synchronized frequency (orange curves). This drop, however, does not extend to zero: $G_D(\nu)$ tends to a finite value when $\nu \rightarrow 0$. Increasing K , G_D develops a more complicated structure: the central region decreases, the tails

grow, and some special values of ν appear, marked by thin gray vertical lines on the figure. They indicate the locations of Ω_- and Ω_+ , defined by $\Omega_{\pm} = \Omega \pm 2a$. The quantities Ω_- , Ω , and Ω_+ are endpoints of intervals which define the integration limits of G_D (see Table II). Since G_D is a piecewise function, the graph of G_D consists of four sub-graphs associated to the intervals $\nu \leq \Omega_-$, $\Omega_- < \nu < \Omega$, $\Omega < \nu < \Omega_+$, and $\Omega_+ \leq \nu$.

In Figures 5 (normal distribution) and 6 (Beta distribution), we compare the distributions of instantaneous, time-averaged and natural frequencies, again for different values of K .

Except for subcritical values of K or near the transition (panels (a) and (b) of each figure), the graphs of \bar{G}_D and G_D are quite different from each other as $\nu \rightarrow \Omega$. In particular while $\bar{G}_D(\nu)$ show a big dip to zero for $K > K_c$, $G_D(\nu)$ approaches non-zero values near the synchronization frequency.

For the Beta distribution (Fig. 6) the tails of \bar{G}_D and G_D reach zero for large enough values of $|\nu|$. As K increases, the support interval shrinks for \bar{G}_D , while it expands for G_D .

B. A focus on tails

The tails of G describe rare events, viz. large instantaneous frequencies with small occurrence probabilities. Here we analyze these events for the Gaussian and Beta cases examined above.

Figure 7 shows the decimal logarithms of G_D (panels (a) and (c)) and \bar{G}_D (panels (b) and (d)) for the normal and Beta distributions studied above, using the same set

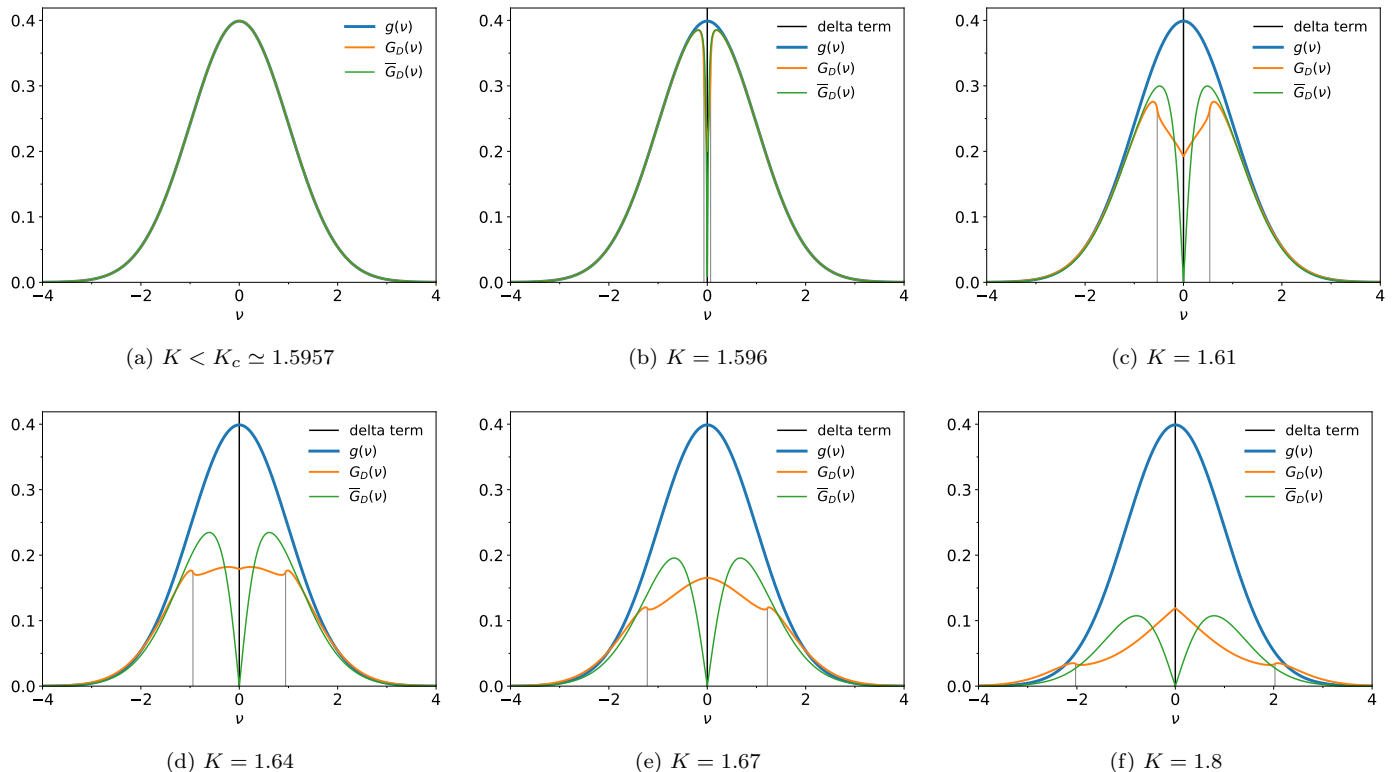


FIG. 5. Comparison between the instantaneous frequency distribution, $G(\nu)$, and the time-averaged frequency distribution, $\bar{G}(\nu)$. A normal distribution of natural frequencies, $g(\nu)$, is assumed. For $K < K_c$, $g(\nu) = G(\nu) = \bar{G}(\nu)$, and there is no delta term, which means that $S(K) = 0$.

of K values as in previous figures.

For clarity, in the Gaussian case, the distributions are plotted as functions of ν^2 , so that Gaussian tails appear as straight lines. For large values of $|\nu|$, the tails of G_D stay above the tails of g , and the difference between $\log[G_D(\nu)]$ and $\log[g(\nu)]$ increases with K . Nevertheless, all G_D distributions keep the same asymptotic tail as g , rescaled by a K -dependent factor (Fig. 7(a)). The tails of \bar{G}_D are also Gaussian, and asymptotically identical but below those of g , rescaled by a K -dependent factor that decreases with K (Fig. 7(c)).

In the case of the Beta distribution, both G_D and \bar{G}_D have a bounded support, and they behave in a qualitatively-similar manner to g near the limit values of their support intervals. The tails of G_D extends beyond the support interval of g , and all the more so as K increases (Fig. 7(b)), while the tails of \bar{G}_D show the opposite tendency (Fig. 7(d)).

Further information about the above results is presented in Figure 8: In panels (a) and (b), we show the decimal logarithms of the ratios G_D/g and \bar{G}_D/g , which shows clearly that G_D “goes away” from g as K increases: in the central region G_D becomes smaller and smaller than g ; in the tails, the difference grows. In comparison, the behavior of \bar{G}_D is much more “gentle”. In the Beta case, we show how the bounds of the support interval

varies with K (Fig 8(c)). For the average frequencies (\bar{G}_D), the support shrinks almost linearly with K , while it grows more slowly than linearly for G_D . Finally, in Fig. 8(d) we show A , the area of G_D beyond the support interval of g . This quantity measures the overall likelihood to observe instantaneous frequencies beyond the possible nominal frequencies. Interestingly, A first grows with K , then decreases, in spite of the monotonous increase of the support of G_D . (In Fig. 7(b), one can understand that this comes from the increasingly trimodal nature of G_D .) We also plot \bar{A} , the area of g outside the support interval of \bar{G}_D , which indicates the overall weight of natural frequencies unobservable as time-averaged frequencies. It increases monotonously with K .

V. RARE EVENTS AND POWER-LAW TAILS

In this section we consider natural frequency distributions with power-law tails and develop a power series expansion of Eq. (51) in order to deepen our understanding of rare events. By rare events we mean occurrences of large instantaneous frequency values such that $\nu \ll \Omega_-$ or $\nu \gg \Omega_+$. We assume that natural frequency distributions are smooth and have unimodal and symmetric profiles centered at $\Omega = 0$.

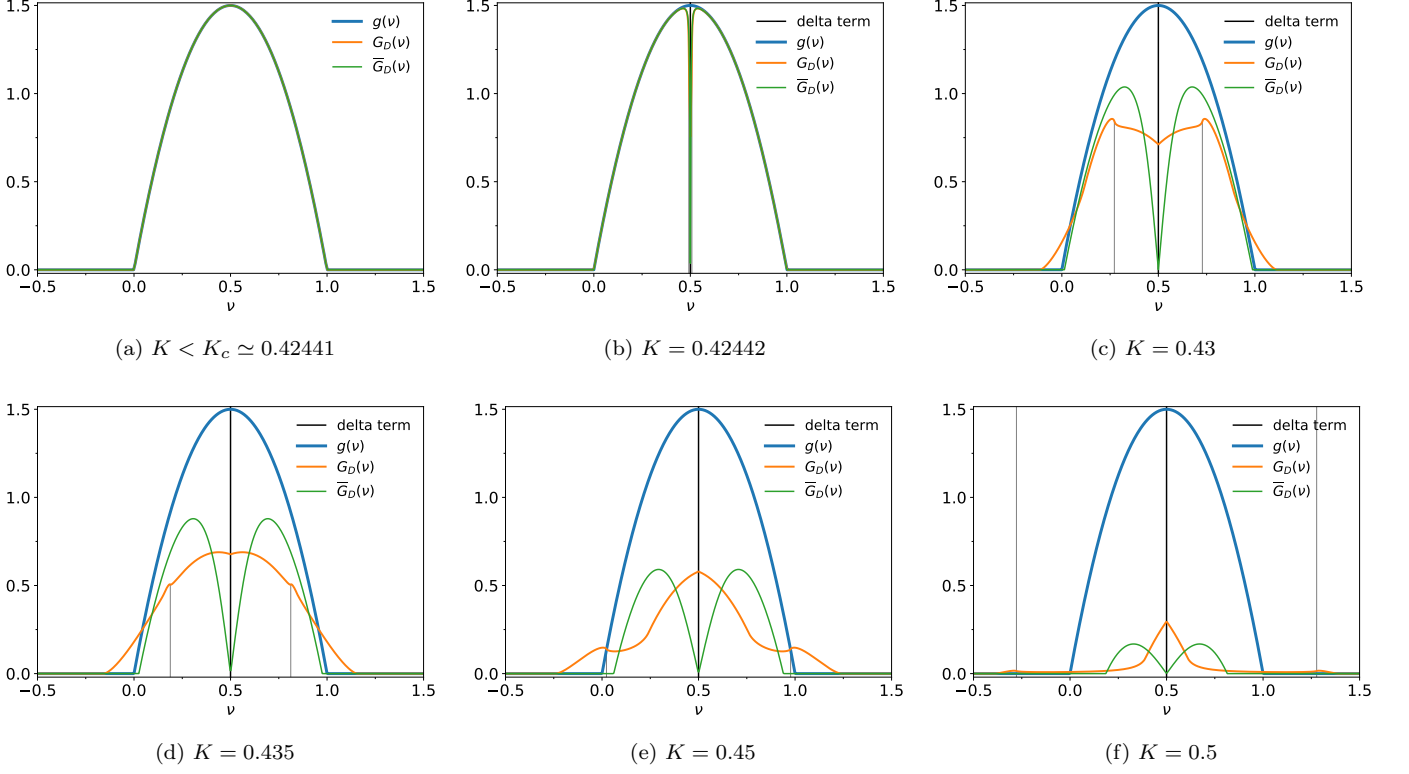


FIG. 6. Comparison between G and \bar{G} . g is a Beta(2,2) distribution. (a) For $K < K_c$, $g(\nu) = G(\nu) = \bar{G}(\nu)$, and there is no delta term, which means that $S(K) = 0$. (b-f) As K increases, the bounding interval of \bar{G} decreases its width, while the bounding interval of $G(\nu)$ becomes larger.

According to Table II, the instantaneous frequency distribution for $\Omega = 0$ and $|\nu| > 2a$ can be written

$$G(\nu) = \frac{1}{\pi|\nu|} \int_{-\frac{\pi}{2}}^{+\frac{\pi}{2}} h(\nu + a \sin \psi) d\psi. \quad (59)$$

with

$$h(x) = u_+(x)g(x)u_-(x) \quad \text{where} \quad u_{\pm}(x) = \sqrt{x \pm a}. \quad (60)$$

Expanding $h(\nu + a \sin \psi)$ as a Taylor series, we have

$$h(\nu + a \sin \psi) = h(\nu) + \sum_{m=1}^{\infty} \frac{a^m}{m!} h^{(m)}(\nu) \sin^m \psi, \quad (61)$$

where $h^{(m)}$ denotes the m th-order derivative of h . Substituting Eq. (61) in Eq. (59), we obtain

$$G(\nu) = \frac{h(\nu)}{|\nu|} + \frac{1}{\pi|\nu|} \sum_{m=1}^{\infty} \frac{a^m}{m!} h^{(m)}(\nu) \int_{-\frac{\pi}{2}}^{+\frac{\pi}{2}} \sin^m \psi d\psi. \quad (62)$$

For any integer $n > 0$, $\int_{-\frac{\pi}{2}}^{+\frac{\pi}{2}} \sin^{2n} \psi d\psi = 2 \int_0^{+\frac{\pi}{2}} \sin^{2n} \psi d\psi$ and $\int_{-\frac{\pi}{2}}^{+\frac{\pi}{2}} \sin^{2n-1} \psi d\psi = 0$. So only even order terms are present in Eq. (62). According to Eq. (3.621-3) in

Ref.[27], $2 \int_0^{+\frac{\pi}{2}} \sin^{2n} \psi d\psi = \pi \frac{(2n-1)!!}{(2n)!!}$, whence

$$G(\nu) = \frac{h(\nu)}{|\nu|} + \frac{1}{|\nu|} \sum_{n=1}^{\infty} \frac{a^{2n}}{(2n)!} \frac{(2n-1)!!}{(2n)!!} h^{(2n)}(\nu). \quad (63)$$

The Leibniz derivative rule allows us to write $h^{(2n)}$ as

$$h^{(2n)}(\nu) = \sum_{k_1+k_2+k_3=2n} \frac{(2n)!}{k_1!k_2!k_3!} \times u_+^{(k_1)}(\nu) g^{(k_2)}(\nu) u_-^{(k_3)}(\nu), \quad (64)$$

where summation is taken over all partitions (k_1, k_2, k_3) of $2n$ into non-negative integers, $g^{(k)}$ and $u_{\pm}^{(k)}$ denote the k th-order derivatives of g . The latter are given by

$$u_{\pm}^{(k)}(\nu) = p_k \left(\frac{1}{2} \right) (\nu \pm a)^{-k} u_{\pm}(\nu), \quad (65)$$

where

$$p_k(q) = \prod_{l=0}^{k-1} (q-l). \quad (66)$$

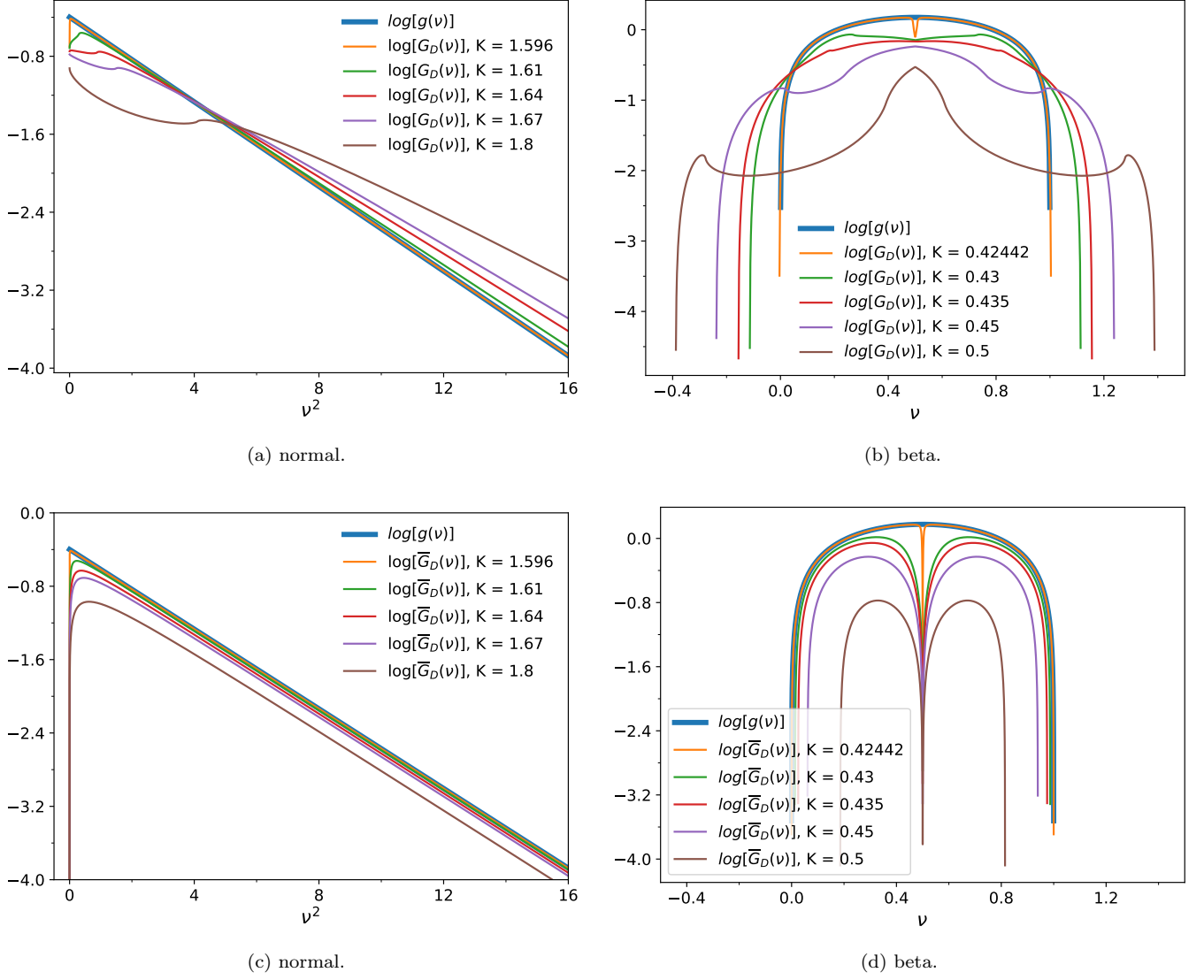


FIG. 7. Decimal logarithms of G_D ($\log[G_D(\nu)]$) and $\bar{G}_D(\nu)$ ($\log[\bar{G}_D(\nu)]$) assuming that g is a normal and a Beta(2, 2) PDF.

From Eqs. (64) and (65), it follows that

$$h^{(2n)}(\nu) = u_+(\nu)u_-(\nu) \sum_{k_1+k_2+k_3=2n} \frac{p_{k_1}(\frac{1}{2})(2n)!p_{k_3}(\frac{1}{2})}{k_1!k_2!k_3!} \times \frac{g^{(k_2)}(\nu)}{(\nu+a)^{k_1}(\nu-a)^{k_3}}. \quad (67)$$

We can now use Eqs. (67), and (60) in Eq. (63) to obtain the ratio $G(\nu)/g(\nu)$, which is given by

$$\frac{G}{g}(\nu) = \sqrt{1 - \left(\frac{a}{\nu}\right)^2} [1 + \Lambda(\nu)], \quad (68)$$

where

$$\Lambda(\nu) = \frac{1}{g(\nu)} \sum_{n=1}^{\infty} c_n(\nu) \left(\frac{a}{\nu}\right)^{2n} \quad (69)$$

and

$$c_n(\nu) = \frac{(2n-1)!!}{(2n)!!} \sum_{k_1+k_2+k_3=2n} \frac{p_{k_1}(\frac{1}{2})p_{k_3}(\frac{1}{2})}{k_1!k_2!k_3!} \times \frac{\nu^{k_2}g^{(k_2)}(\nu)}{\left(1 + \frac{a}{\nu}\right)^{k_1} \left(1 - \frac{a}{\nu}\right)^{k_3}}. \quad (70)$$

(If g is centered at a non-zero synchronization frequency Ω , more general formulas than Eqs. (68), (69), and (70) can be obtained by changing in them the terms $\frac{a}{\nu}$ by $\frac{a}{(\nu-\Omega)}$.)

As an application of the result given by (68), let us now consider a class of natural frequency distributions of the form

$$g(\nu) \sim C\nu^{-2\mu} \quad (|\nu| \rightarrow \infty), \quad (71)$$

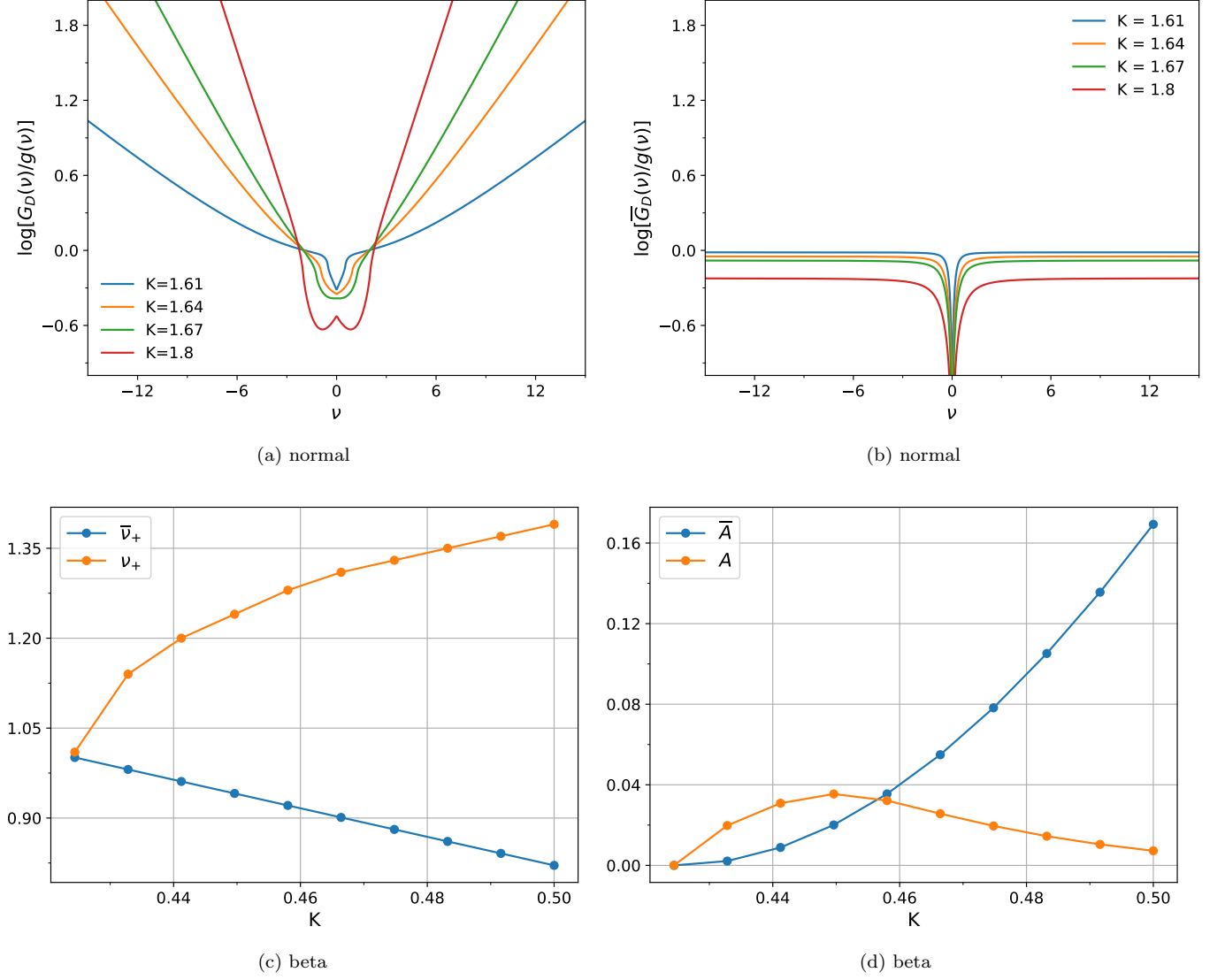


FIG. 8. (a) Decimal logarithms of the ratio $\frac{G(\nu)}{g(\nu)}$: as ν increases, $\frac{G(\nu)}{g(\nu)}$ diverges. (b) Decimal logarithms of $\frac{\bar{G}(\nu)}{g(\nu)}$ remains constant as ν increases. (c) Positive endpoints of the support intervals of G and \bar{G} , denoted by ν_+ and $\bar{\nu}_+$. (d) Area of G outside the support interval of g (A), and area of g outside the support interval of \bar{G} (\bar{A}).

where μ is a positive integer, and C a real constant.

Its derivatives read

$$g^{(k)}(\nu) \sim p_k (-2\mu) \nu^{-k} g(\nu) \quad (|\nu| \rightarrow \infty), \quad (72)$$

where p_k is given by Eq. (66), and $k = 0, \dots, 2n$. Since $(1 \pm \frac{a}{\nu})^k \sim 1$ as $|\frac{a}{\nu}| \rightarrow 0$, it follows from (70) and (72) that

$$c_n(\nu) \sim \bar{c}_n g(\nu) \quad \left(\left| \frac{a}{\nu} \right| \rightarrow 0 \right), \quad (73)$$

where the constant coefficient \bar{c}_n is defined by

$$\bar{c}_n = \frac{(2n-1)!!}{(2n)!!} \sum_{k_1+k_2+k_3=2n} \frac{p_{k_1}(\frac{1}{2}) p_{k_2}(-2\mu) p_{k_3}(\frac{1}{2})}{k_1! k_2! k_3!}. \quad (74)$$

Therefore,

$$\Lambda(\nu) \Big|_{\frac{a}{\nu} \rightarrow 0} \sim \sum_{n=1}^{\infty} \bar{c}_n \left(\frac{a}{\nu} \right)^{2n}, \quad (75)$$

and

$$\frac{G}{g}(\nu) \Big|_{\frac{a}{\nu} \rightarrow 0} \sim \sqrt{1 - \left(\frac{a}{\nu} \right)^2} \left\{ 1 + \bar{c}_1 \left(\frac{a}{\nu} \right)^2 + O \left[\left(\frac{a}{\nu} \right)^4 \right] \right\}. \quad (76)$$

This means: assuming that $g(\nu)$ has power-law tails of form (71), $G(\nu)$ approaches asymptotically $g(\nu)$ for large instantaneous frequencies (compared to a) or small order parameter values (compared to $|\frac{K}{\nu}|$).

To illustrate this point, we consider the family of nat-

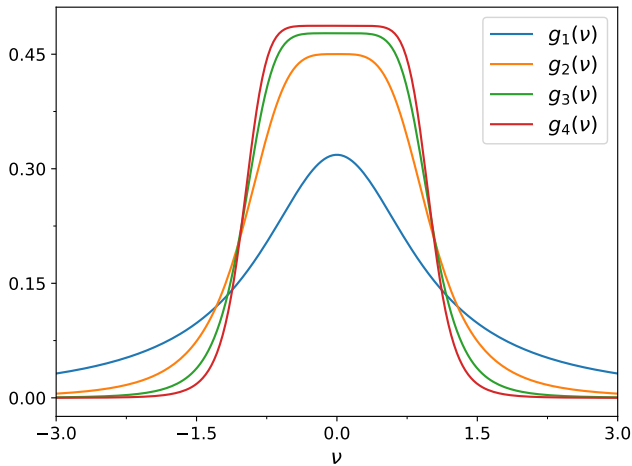


FIG. 9. Graphs of g_μ , defined by (77), for $\mu = 1, 2, 3, 4$.

ural frequency distributions

$$g_\mu(\nu) = \frac{\mu}{\pi(1 + \nu^{2\mu})} \sin\left(\frac{\pi}{2\mu}\right), \quad (77)$$

where μ is a positive integer. Formula (77) generalizes the standard Cauchy-Lorentz distribution, which corresponds to the particular case g_1 . Graphs of $g_\mu(\nu)$ are shown in Fig. 9 for $\mu = 1, 2, 3, 4$. By increasing μ , the tails of $g_\mu(\nu)$ gets thinner, and high natural frequencies have lower occurrence probabilities. In Figs. 10(a)-(d), we show graphs of \overline{G}_D and G for different values of K considering the cases g_1 and g_3 .

Figures 11(a) and (c) show decimal logarithms of the ratio \overline{G}_D/g , where $\overline{G}_D(\nu)$ is computed using Eq. (17) with $g(\nu) = g_\mu(\nu)$. Like in the Gaussian and Beta examples of Sec. IV, the graphs of \overline{G}_D are more and more below the graph of g as increasing K increases. Yet, for $|\nu| \rightarrow \infty$, $\overline{G}_D(\nu)$ and $g(\nu)$ show the same asymptotic behavior.

In Figs. 11(b) and (d), we show decimal logarithms of the ratio G/g for the same K values used in Figs. 11(a) and (c). All graphs show that $\log[\frac{G}{g}(\nu)] \rightarrow 0$ as $|\frac{a}{\nu}| \rightarrow 0$, which is in agreement with formula (76). So $G(\nu)$ converges to $g(\nu)$ as ν increases, albeit this convergence is restrained by increasing K .

Another somewhat counterintuitive effect is related to the tail thickness of g_μ . Compared to the other distributions $g_{\mu>1}$, g_1 decays more slowly as ν increases, and $\log[\frac{G}{g_1}(\nu)]$ decays more easily to zero. When μ increases, g_μ 's tails become thinner, and convergence of $\log[\frac{G}{g_\mu}(\nu)]$ to zero requires larger values of ν . A simple explanation to this tail thickness effect is related to the critical order parameter, which is defined by $K_c^{(\mu)} = \frac{2}{\pi g_\mu(0)}$, if $g = g_\mu$ (see Eq. (7)). Since the normalization condition remains valid for any μ , thinner tails result in higher $g(0)$. If $g_\mu(0) > \dots > g_2(0) > g_1(0)$, then $K_c^{(\mu)} < \dots < K_c^{(2)} < K_c^{(1)}$. So, for K fixed, the dif-

ference $K - K_c^{(\mu)}$ decreases with decreasing μ , R (and a) diminishes, and G resembles more closely g_μ . When R is small, $G(\nu)$ converges more easily $g_\mu(\nu)$ as $|\frac{a}{\nu}| \rightarrow 0$. This is shown by Eq. (76) and Figs. 11(b) and (d).

VI. CONCLUSION

Based on Kuramoto theory, we have obtained an analytical formulation of the instantaneous frequency distribution in the Kuramoto model. Numerical data show excellent agreement with our formula, provided they are obtained on very large collections of oscillators studied in their steady state (see Appendix), i.e. in the limits where our results are expected to be valid. Access to the distribution of instantaneous frequencies G extends Kuramoto theory, which was limited heretofore to the knowledge of \overline{G} , the distribution of time-averaged, or ‘‘coupling-modified’’, frequencies.

Distributions G and \overline{G} are functionals of the natural frequency distribution g . Irrespective of g , the synchronization scenario keeps the same basic features: beyond the critical coupling strength value $K_c = \frac{2}{\pi g(\Omega)}$, a subset of oscillators synchronize, so that both \overline{G} and G comprise a delta peak at the frequency Ω . This delta peak is identical for both G and \overline{G} and represents the fraction of synchronized oscillators, which grows monotonously with K (at least for the g distributions considered here, see e.g. Fig. 4). As soon as $K > K_c$, the continuous part of both G and \overline{G} departs from g . Whereas \overline{G} remains below g everywhere, and displays a characteristic dip near the synchronized frequency Ω , the continuous part of G has tails that pass over g and shows a maximum at Ω for K large enough. This last fact reflects the relaxation-oscillation-like dynamics of oscillators with natural frequency outside but close to the synchronization band.

The distribution of instantaneous frequencies G typically displays a rather complicated structure. It is in fact trimodal for K large enough, even as the natural frequency distributions considered here are unimodal. Nevertheless, from the 3 qualitatively-different examples of g studied here, we have shown that G , like \overline{G} , displays the same tails as g : a normal g yields Gaussian tails for G and \overline{G} which are just rescaled versions of those of g . For a Beta g with a bounded support interval, G and \overline{G} both have bounded supports, respectively wider and narrower than that of g .

Due to the difficulty in extracting explicit expressions from our results, most of the information about the distribution of instantaneous frequencies presented here has been obtained by numerical analysis of our formula. Yet, when dealing with rare events in the example of powerlaw tailed distribution of natural frequencies, a power-series analysis of the distribution of instantaneous frequencies has allowed us to obtain an asymptotic expansion in frequency. This has confirmed that g , G , and \overline{G} are asymptotically equivalent in the limit of large frequencies.

Beyond their intrinsic interest for a deeper understand-

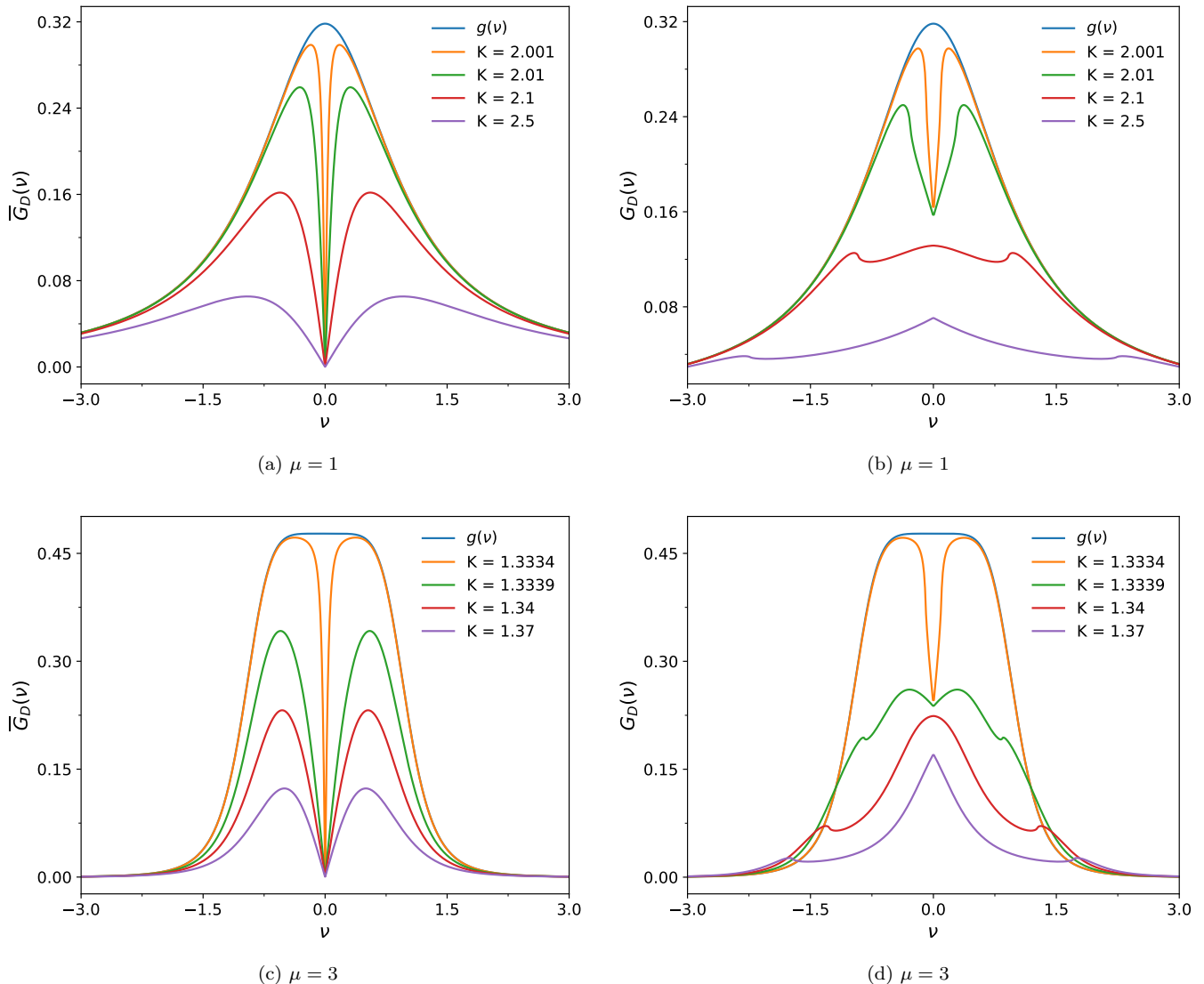


FIG. 10. \bar{G}_D and G for $g = g_\mu$, defined by (77).

ing of synchronization, our results are useful when it comes to choosing a numerical scheme and resolution to simulate coupled oscillators: indeed a faithful simulation must account properly for the largest instantaneous frequencies displayed by the system. As seen and quantified here, these are larger than the largest natural frequency present, which implies, e.g., to choose higher-order integration schemes and/or smaller timesteps than naively suggested by the natural frequencies at play.

The approach followed here can easily be extended to non-symmetric and/or non-unimodal distributions of natural frequencies. We also believe that important variants of the Kuramoto model, such as the Kuramoto-Sakaguchi model [15] are amenable to the same type of analysis as developed here. More generally, we hope that this work opens new perspectives on synchronization phenomena beyond the usual order-parameter analysis.

ACKNOWLEDGMENTS

This work was made possible through financial support from Brazilian research agency FAPESP (grant n. 2019/12930-9). JDF warmly thanks Prof. Joao Peres for valuable discussions. EDL thanks support from Brazilian agencies CNPq (301318/2019-0) and FAPESP (2019/14038-6).

Appendix: Numerical checks

In this section we validate the formula of G_D against numerical results from simulations of the Kuramoto model. Our check is restricted to the Gaussian and Beta examples discussed of Sec. IV. Simulations were performed with the numerical library ODEPACK [28]. The

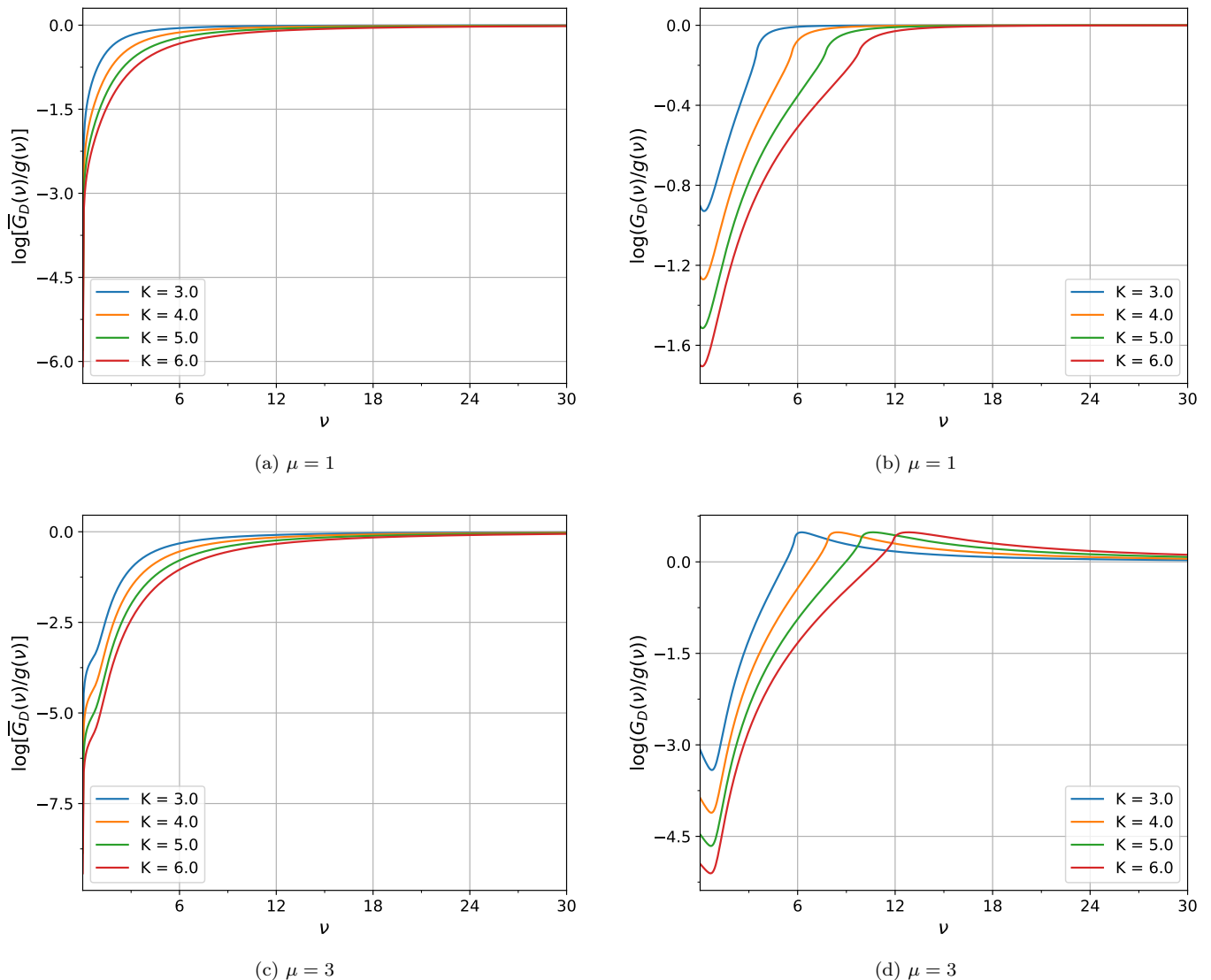


FIG. 11. Decimal logarithms of the ratios $\frac{\bar{G}_D}{g}(\nu)$ and $\frac{G_D}{g}(\nu)$. $g(\nu) = g_\mu(\nu)$, defined by Eq. (77).

ODEPACK's solver used in all simulations was *LSODA*, an hybrid implementation of Adams and BDF methods [29].

1. Gaussian case

In Figs. 12(a)-(f), we compare graphs of G_D , the same shown in Fig. 4, to numerically-obtained normalized histograms of the instantaneous frequencies.

The histograms were obtained from numerical simulations of the Kuramoto model with $N = 5 \times 10^5$. In all simulations, the Kuramoto system of equations is numerically integrated from an initial time $t_0 = 0$ to a final time $t_f = 5 \times 10^2$. Each histogram is created from the set of instantaneous frequencies $\{\hat{\theta}_i(t_f)\}_{i=1}^N$. Simulations

are performed considering random samples of natural frequencies and initial phases. Initial phases are uniformly sampled: a sample $\{\theta_i(t_0)\}_{i=1}^N$ is generated according to a uniform distribution in the interval between 0 and 2π .

Figure 13 shows the typical evolution of the numerical order parameter. When the order parameter exhibits small fluctuations after a sufficiently long time, the corresponding histograms are in good agreement with the analytical curves. However, stronger order parameter fluctuations are observed near the transition ($K = 1.596$), and the histogram shown in Fig. 12(b), obtained with the same value of K , does not fit properly the curve.

Figures 14(a) and 14(b) show, in logarithmic scale, the graph of G_D and histograms of instantaneous frequencies obtained from simulation data. The coupling strength has the same value used in Fig. 12(d), $K = 1.64$. The histograms are created with $N = 5 \times 10^5$ (Fig. 14(a))

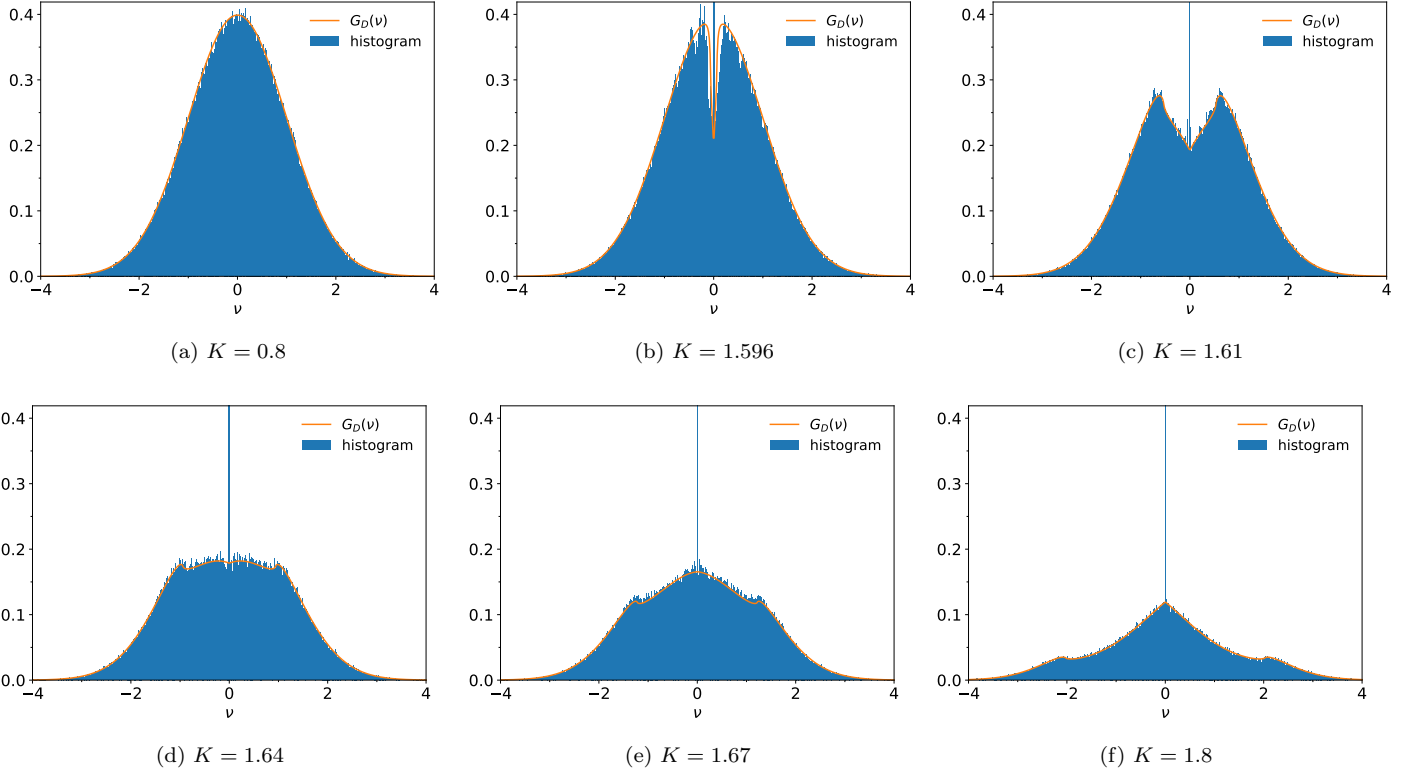


FIG. 12. Comparison between normalized histograms of instantaneous frequencies (in blue), obtained from numerical simulations of the Kuramoto model, and the curve of G_D (in red). In all simulation, $N = 5 \times 10^5$.

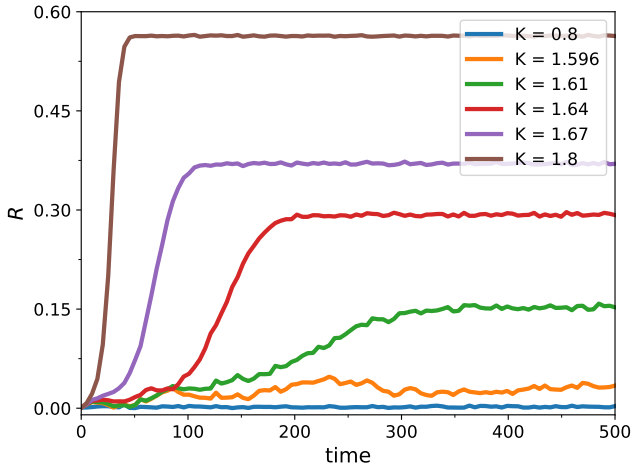


FIG. 13. Time-dependence of the numerical order parameter. Except near the transition, where $K = 1.596$, low fluctuations are observed after a sufficiently long time. Created with the same simulation near the transition, histogram of Fig. 12(b) does not fit properly the theoretical curve.

and $N = 5 \times 10^6$ (Fig. 14(b)). In both of them, the synchronization peak is clearly visible. Large instantaneous frequency occurrences (rare events) are more difficult to observe. However, by increasing the number of oscilla-

tors, rare events are more common, and the tails of G_D fit better the histograms.

2. Beta case

In Figs. 15(a)-(f), we compare instantaneous frequency histograms to graphs of G_D with g defined as the Beta(2,2) distribution, given by Eq. (58). Simulations were performed with $N = 1 \times 10^6$ oscillators, and integration time was 2×10^3 . Histograms were created by using the instantaneous frequency set $\{\hat{\theta}_i(t_f)\}_{i=1}^N$. Corresponding time series of the numerical order parameter are shown in Fig. 16. Similarly to the case of normally-distributed natural frequencies, stronger order-parameter fluctuations are observed near the transition ($K = 0.42442$), away from which our analytical result describes better the histograms.

Behavior near the tails is shown in Fig. 17, where we compare again G_D to instantaneous frequency histograms. The vertical axis has logarithmic scale for values greater than 10^{-4} and linear scale between 0 and 10^{-4} . We use the same coupling strength as in Fig. 15(d). As expected: i) rare events cannot be easily observed in the histograms; ii) by increasing the number of oscillators from $N = 1 \times 10^6$ to $N = 2 \times 10^6$, these events are more common, and a better fit is attainable in the tails.

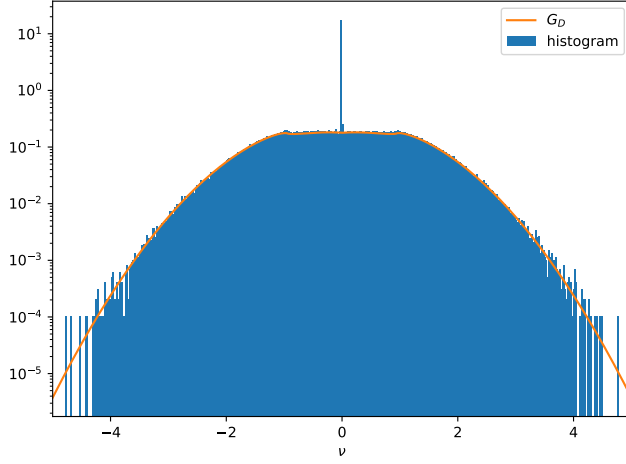
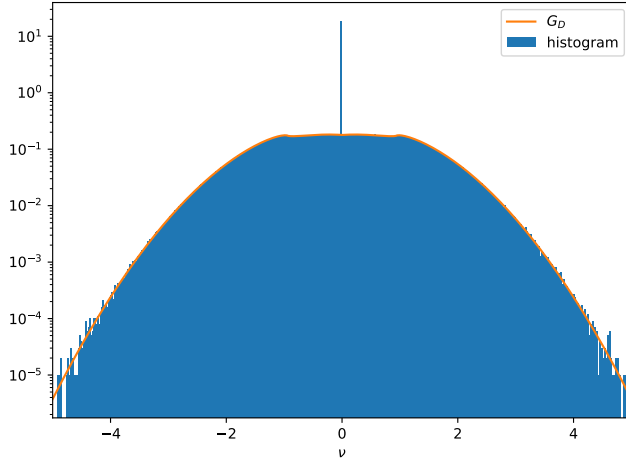
(a) $N = 5 \times 10^5$; $K = 1.64$ (b) $N = 5 \times 10^6$; $K = 1.64$

FIG. 14. Comparison (in logarithmic scale) between the graph of G_D and histograms of instantaneous frequencies. The tails of G_D fit better the histograms when network size increases from $N = 5 \times 10^5$ to $N = 5 \times 10^6$.

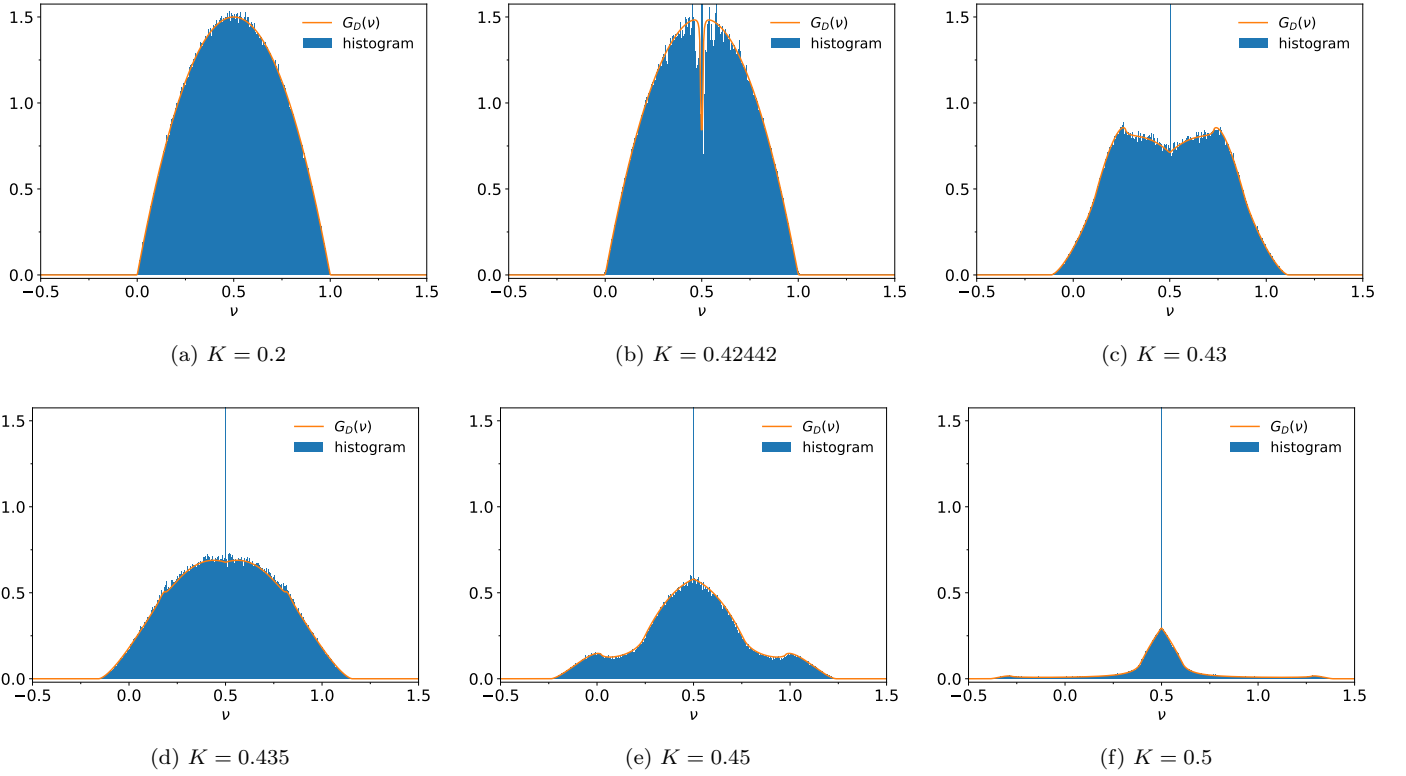


FIG. 15. Comparison of G_D graphs to instantaneous frequency histograms. g is a Beta(2,2) distribution, and the histograms were obtained from simulations of the Kuramoto model with $N = 1 \times 10^6$. The graphs provide better fits than near the transition ($K = 0.42442$).

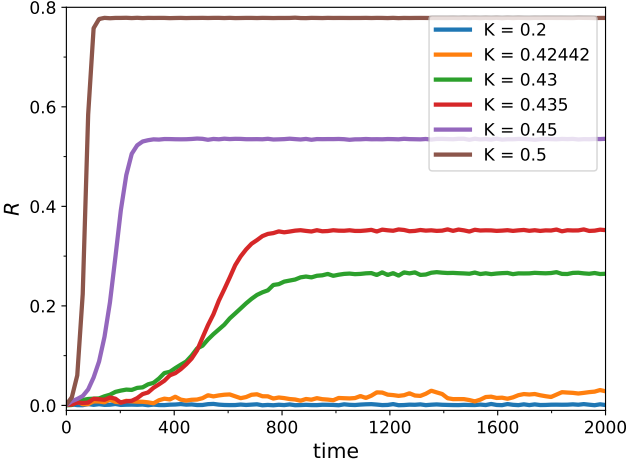
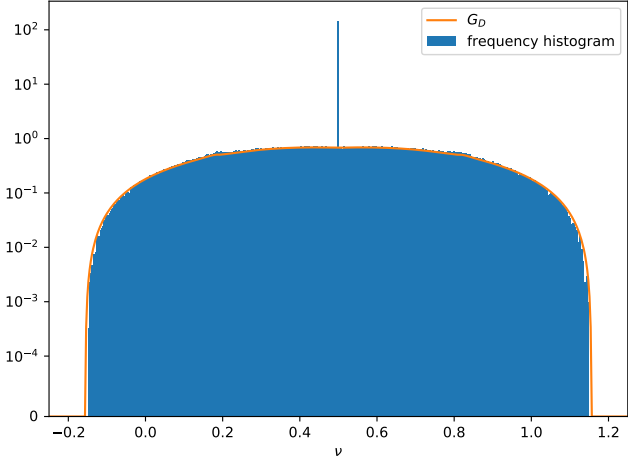
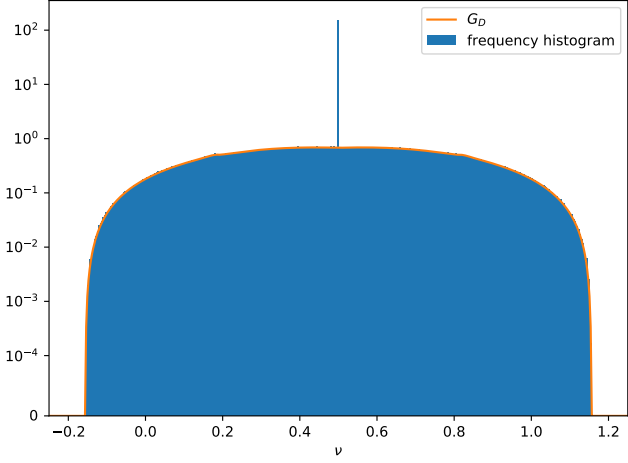


FIG. 16. Time-dependence of the numerical order parameter: low fluctuations after long time, except near the synchronization transition.



(a) $N = 10^6$; $K = 0.435$



(b) $N = 2 \times 10^6$; $K = 0.435$

FIG. 17. Graph of G_D and instantaneous frequency histograms. For the vertical axis, we use logarithmic scale for values greater than 10^{-4} and linear scale those between 0 and 10^{-4} . By increasing the number of oscillators, a better fit is attainable in the tails.

-
- [1] A. Pikovsky, M. Rosenblum, and J. Kurths, *Synchronization, A Universal Concept in Nonlinear Sciences* (Cambridge University Press, Cambridge, 2001).
- [2] M. Breakspear, S. Heitmann, and A. Daffertshofer, *Front. Human Neurosci.* 4, 190 (2010).
- [3] G. Kozyreff, A. G. Vladimirov, and P. Mandel, *Phys. Rev. Lett.* 85, 3809 (2000).
- [4] A. T. Winfree, *The Geometry of Biological Times* (Springer, New York, 1980).
- [5] A. E. Motter, S. A. Myers, M. Anghel, and T. Nishikawa, *Nat. Phys.* 9, 191 (2013).
- [6] M. Bier, B. M. Bakker, and H. V. Westerhoff, *Biophys. J.* 78, 1087 (2000).
- [7] K. Wiesenfeld, P. Colet, and S. H. Strogatz, *Phys. Rev. Lett.* 76, 404 (1996).
- [8] I. Z. Kiss, Y. Zhai, and J. L. Hudson, *Science* 296, 1676 (2002).
- [9] A. T. Winfree, *J. Theor. Biol.* 16, 15 (1967).
- [10] Y. Kuramoto, *International Symposium on Mathematical Problems in Theoretical Physics*, edited by H. Araki, *Lecture Notes in Physics No. 30* (Springer, New York, p. 420).
- [11] Y. Kuramoto, *Chemical Oscillations, Waves and Turbulence* (Springer-Verlag, Berlin, 1984).
- [12] Y. Kuramoto, *Progr. Theoret. Phys. Suppl.* 79, 223 (1984).
- [13] Y. Kuramoto, and I. Nishikawa, *J. Statist. Phys.* 49, 569 (1987).
- [14] Y. Kuramoto, and I. Nishikawa, *Cooperative Dynamics in Complex Physical Systems*, edited by H. Takayama (Springer, Berlin, 1989, p. 300).
- [15] H. Sakaguchi, Y. Kuramoto, *Progr. Theoret. Phys.* 76, 576 (1986).
- [16] H. Sakaguchi, *Prog. Theor. Phys.* 79, 39 (1988).
- [17] C. A. Moreira and M. A. M. de Aguiar, *Physica A* 514, 487 (2019).
- [18] M. Komarov and A. Pikovsky, *Physica D* 289, 18 (2014).
- [19] H. Hong, H. Chate, L. H. Tang, and H. Park, *Phys. Rev. E* 92, 022122 (2015).
- [20] F. A. Rodrigues, T. K. D. Peron, P. Ji, and J. Kurths, *Phys. Rep.* 610, 1 (2016).
- [21] J. D. da Fonseca, and C.V. Abud, *Journal of Statistical Mechanics: Theory and Experiment*, 103204 (2018).
- [22] L. Basnarkov and V. Urumov, *Phys. Rev. E* 78, 011113 (2008).
- [23] Y. Terada, K. Ito, T. Aoyagi and Y. Y. Yamaguchi, *J. Stat.Mech.* (2017) 013403.
- [24] D. T. Gillespie, *American Journal of Physics* 51, 520 (1983).
- [25] R. T. Seeley, *Distributions on Surfaces*, Report TW 78, *Mathematisch Centrum, Amsterdam* (1962).
- [26] E. M. De Jager, *Applications of Distributions in Mathematical Physics* (Amsterdam, *Math. Centre Tract* 10, 1969).
- [27] S. Gradshteyn and I. M. Ryzhik, *Table of Integrals, Series, and Products* (Academic Press, New York, 2007).
- [28] A. C. Hindmarsh, "ODEPACK, A Systematized Collection of ODE Solvers," *IMACS Transactions on Scientific Computation*, Vol 1., pp. 55-64, 1983.
- [29] L. Petzold, *SIAM Journal on Scientific and Statistical Computing*, Vol. 4, No. 1, pp. 136-148, 1983.
- [30] For the sake of simplicity, here we always use the terms "distribution" or "PDF" when referring to a probability density function.
- [31] Our opinion is that there are few works based on Kuramoto theory discussing asymmetry effects of the natural frequency distribution, such as, for example, Refs. [22, 23]. Eq. (6) or alternative equivalent forms are more commonly used.